Inhibition of the acetyltransferase NAT10 normalizes progeric and aging cells by rebalancing the Transportin-1 nuclear import pathway

Authors: Delphine Larrieu[1,2]*, Emmanuelle Viré[1,3Ψ], Samuel Robson[1,4Ψ], Sophia Y. Breusegem[2], Tony Kouzarides[1] and Stephen P. Jackson[1]*

Affiliations:

[1] The Wellcome Trust/Cancer Research UK Gurdon Institute and Department of Biochemistry, University of Cambridge, CB2 1QN, United Kingdom.

[2] Current address: Cambridge Institute for Medical Research, Department of clinical biochemistry, University of Cambridge, CB2 0XY, United Kingdom

[3] Current address: MRC Prion Unit at UCL, Institute of Prion Diseases, Queen Square House, Queen Square London, WC1N 3BG, United Kingdom

[4] Current address: School of Pharmacy & Biomedical Science, University of Portsmouth, PO1 2UP, United Kingdom

* Corresponding authors. Email: dl437@cam.ac.uk or s.jackson@gurdon.cam.ac.uk

[Ψ] These authors contributed equally to the work.

ABSTRACT

Hutchinson-Gilford progeria syndrome (HGPS) is an incurable premature ageing disease. Identifying deregulated biological processes in HGPS might thus help define novel therapeutic strategies. Fibroblasts from HGPS patients display defects in nucleo-cytoplasmic shuttling of the GTP-bound form of the small GTPase Ran (RanGTP), which leads to abnormal transport of proteins into the nucleus. Here, we report that microtubule stabilisation in HGPS cells sequestered the non-classic nuclear import protein Transportin-1 (TNPO1) in the cytoplasm, thus affecting the nuclear localisation of its cargos, including the nuclear pore protein NUP153. Consequently, nuclear Ran, nuclear anchorage of the nucleoporin TPR, and chromatin organisation were disrupted, deregulating gene expression and inducing senescence. Inhibiting N-acetyltransferase 10 (NAT10) ameliorated HGPS phenotypes by rebalancing the nuclear to cytoplasmic ratio of TNPO1. This restored nuclear pore complex integrity and nuclear Ran localisation, thereby correcting HGPS cellular phenotypes. We observed a similar mechanism in cells from healthy aged individuals. This study identifies a nuclear import pathway affected in ageing and underscores the potential for NAT10 inhibition as a possible therapeutic strategy for HGPS, and perhaps also for pathologies associated with normal ageing.

INTRODUCTION

Hutchinson-Gilford progeria syndrome (HGPS) is a very rare, fatal premature ageing syndrome caused by a *de novo* heterozygous point mutation within exon 11 of the *lamin A* (*LMNA*) gene (1,2). *LMNA* encodes two type V intermediate filament proteins: lamin A and lamin C. Together with B-type lamins, these proteins form the nuclear lamina at the inner nuclear membrane, where they act as a scaffold to maintain nuclear architecture, nuclear pore complexes, and chromatin organisation, and to regulate DNA replication and transcription. In HGPS, the mutation only affects lamin A and causes the production of a truncated, toxic form of the protein called progerin that acts as a dominant negative. Accumulation of progerin at the inner nuclear membrane alters nuclear lamina structure, causing abnormal nuclear morphology, aggregation of nuclear pore complexes, chromatin disorganisation due to loss of peripheral heterochromatin anchorage, and transcriptional deregulation, all of which ultimately lead to DNA damage accumulation and premature entry of HGPS cells into senescence (3-6). These cellular phenotypes are also observed in cells from healthy aged individuals. In HGPS patients, progerin accumulation triggers segmental premature ageing, in which most tissues are affected but the patient displays only some of the phenotypes typical of normal aging, usually starting within the first year of life and leading to death at the average age of 14, mainly due to heart defects (7,8). Although HGPS syndrome was first described over a century ago, the exact mechanisms by which progerin drives such striking cellular and organismal phenotypes are still being explored.

Various studies have reported disruption of nucleocytoplasmic transport in HGPS fibroblasts, due to an abnormal nucleocytoplasmic gradient of GTP-bound Ran (RanGTP) (9-11). Ran is a small GTPase that shuttles between the cytoplasm and the nucleus and cycles between GDP-bound and GTP-bound states (12), with conversion between these states being

catalysed by cytoplasmic factors, such as Ran GTPase-activating protein (RanGAP) (13), and nuclear factors, such as the regulator of chromatin condensation 1 (RCC1) (14,15). Therefore, Ran is predominantly in its GTP-bound form in the nucleus, and in its GDP-bound form in the cytoplasm. This creates a RanGTP gradient across the nuclear envelope (16,17), which allows active transport of protein cargoes through nuclear pore complexes by a family of carrier proteins called karyopherins. In HGPS, the presence of progerin induces defects in Ran nuclear localisation. Consequently, nuclear import of proteins requiring Ran-dependent active transport through nuclear pores appeared more strongly affected than that of proteins passively diffusing through nuclear pores in these cells. One of the proteins displaying reduced nuclear import in HGPS cells is the nucleoporin translocated promoter region (TPR) (9,10), a polypeptide of ~265 kDa that forms a homodimer and is thus one of the largest nucleoporins. TPR is the last protein recruited to the nuclear pore complex, and its anchorage in the nuclear envelope requires the nuclear pore protein NUP153 (18,19). We previously showed that disrupting NUP153 abundance or function affects Ran nuclear localisation, thus impairing nuclear import of p53-binding protein 1 (53BP1), which is involved in DNA damage repair. This contributes to DNA damage accumulation in ageing vascular smooth muscle cells (VSMCs) (20). Remodelin, a small-molecule inhibitor of N-acetyltransferase 10 (NAT10) that normalises phenotypes of fibroblasts isolated from HGPS patients (21), restores NUP153 localisation and nuclear Ran in VSMCs through an uncharacterised mechanism (20). This raises the question of why the abundance of nuclear Ran is altered in HGPS cells and which aspect of nuclear transport machinery is disrupted, because NUP153 can be imported by several import pathways (22-24).

Here we show that the decrease of nuclear Ran abundance that occurs in cells from HGPS patients and in cells from aged individuals is linked to dysregulation of the non-classic

4

transport pathway mediated by Transportin-1 (TNPO1), also called karyopherin β2 (25).

Unlike classical importin proteins, which are general transporters, TNPO1 only mediates the

nuclear import of a subset of proteins. In the nucleus, RanGTP binds to TNPO1 to stimulate

release of the cargo (26). Among TNPO1 cargos, the most extensively characterised is the

RNA-binding protein heterogeneous nuclear ribonucleoprotein 1 hnRNPA1 (27), which

functions in several processes including mRNA biogenesis and promotion of transcription

factor activity (28-30). Nuclear pore complex protein NUP153 is also a target for TNPO1-

mediated nuclear import (24). Accordingly, we observed that hnRNPA1, NUP153, TPR, and

nuclear Ran defects in HGPS cells were linked to deregulation of the TNPO1 nuclear-to-

cytoplasmic ratio. NAT10 inhibition restored the proper subcellular distribution of TNPO1

and TNPO1-dependent nuclear import in HGPS cells, thereby promoting nuclear localisation

of its cargos such as hnRNPA1 and NUP153. This allowed proper NUP153-dependent

recruitment of TPR to the nuclear pore complex and restored chromatin reorganisation and

global gene transcription, thus preventing premature entry of HGPS cells into senescence.

NUP153 depletion did not affect the TNPO1 pathway, supporting the notion that TNPO1

deregulation in HGPS is the cause and not the consequence of abnormal NUP153 nuclear

localisation. This study thus provides mechanistic insight into how NAT10 inhibition

reverses HGPS cellular phenotypes and provides further evidence that it may also be relevant

in normal ageing.

RESULTS

Premature ageing and normal aged cells display nucleocytoplasmic transport defects

We found by immunofluorescence staining that, as expected (31), most Ran was in the nuclei of interphase fibroblasts from a healthy 20-year-old individual (Fig. 1A). By contrast, and in line with previous reports (9,10), we observed that Ran localization was abnormal in fibroblasts from an HGPS patient (HGPS 11513), with most Ran being cytoplasmic (Fig. 1A). Because evidence suggests that HGPS might recapitulate various aspects of normal ageing (32), we also looked at the subcellular localisation of Ran in fibroblasts from healthy individuals between 81 and 96 years-of-age (AG11240, AG04059, AG05248, and AG09602). Similarly to HGPS cells, nuclear Ran appeared to be depleted to various extents in cells from aged individuals (Fig. 1A). This reduction in nuclear Ran was not associated with an overall decrease in Ran abundance in fibroblasts from the HGPS patient or in fibroblasts from aged individuals (Fig. 1B), suggesting that changes in Ran subcellular localisation reflected dysregulated RanGTP gradient formation across the nuclear envelope rather than changes in Ran abundance. As reported previously (10), decreased nuclear Ran in HGPS cells was also associated with decreased nuclear staining intensity of the nucleoporin TPR (Fig. 1C, D) as well as in cells from aged healthy individuals (Fig. S1A, B). These results confirmed previous findings in HGPS cells and also suggested that a similar nucleo-cytoplasmic transport defect may occur during normal ageing.

Inhibition of NAT10 restores normal nucleocytoplasmic transport in HGPS cells

Because the nuclear pore complex protein NUP153 is required to anchor TPR to the nuclear pore complex (18), we assessed whether NUP153 was present at the nuclear periphery by immunofluorescence in fibroblasts from control individuals and from HGPS patients (hereafter referred to as control or unaffected and HGPS fibroblasts, respectively). NUP153

nuclear intensity was significantly reduced in HGPS cells compared to controls, in a manner that correlated with decreased nuclear TPR staining (Fig. 1E, F and Fig. S2A). Because we had previously reported that inhibition of the N-acetyltransferase NAT10 reverses abnormal phenotypes of HGPS cells as well as aged smooth-muscle cells (20,21), we investigated whether NAT10 inhibition affected NUP153 and TPR staining. Indeed, when we treated HGPS cells with the NAT10 inhibitor Remodelin (21), this increased the nuclear staining intensity of NUP153 and TPR (Fig. 1E, F). To assess whether this reflected an enhanced interaction between the NUP153 and TPR proteins after Remodelin treatment, we performed a proximity ligation assay (PLA) (33) using primary antibodies recognizing TPR and NUP153. Whereas NUP153 and TPR clearly interacted in control fibroblasts (Fig. 1G), the interaction was almost completely absent in untreated HGPS cells, in accord with these proteins being mislocalised. However, Remodelin treatment greatly enhanced the interaction between NUP153 and TPR in HGPS cells (Fig. 1G). This suggested that NAT10 inhibition promoted normal nuclear localisation and anchorage of both NUP153 and TPR at the nuclear periphery of HGPS cells.

We next looked at the effect of NAT10 inhibition on Ran subcellular localisation in HGPS cells. Strikingly, short-interfering RNA (siRNA)-mediated depletion of NAT10, or NAT10 inhibition by Remodelin nearly completely abolished Ran nuclear localisation defects in HGPS cells (Fig. 1H, I, Fig. S2B). In agreement with nuclear transport factor 2 (NTF2) mediating Ran nuclear import (34,35), siRNA depletion of NTF2 in control fibroblasts reduced Ran nuclear accumulation, similar to that observed in untreated HGPS cells (Fig. 1H, I).

Reduction of nuclear Ran modifies chromatin compaction and triggers senescence

Because many cellular processes are disrupted in HGPS, we explored which might be associated with decreased nuclear Ran abundance. One of the phenotypes observed in HGPS cells is chromatin disorganisation and loss of heterochromatin marks, including trimethylation of histone H3 at lysine 9 (H3K9me3) (36,37). To assess whether disrupting Ran nuclear import could affect the state of chromatin at a global level, we transfected non-progeric human bone osteosarcoma U2OS cells with siRNA targeting NTF2 (Fig. 2A) and looked at global chromatin compaction by treating nuclei harvested from these cells with micrococcal nuclease (MNase). The efficiency of MNase digestion varies with the degree of chromatin compaction. We used U2OS cells for this experiment instead of primary human cells because this assay requires a large number of cells. These assays established that disruption of nuclear Ran localisation led to global chromatin decompaction (Fig. 2B) and suggested that, by affecting the bi-directional transport of many large cargo proteins, Ran deregulation might have broad effects on chromatin organisation, as observed in HGPS (36,37). Chromatin relaxation was also observed – albeit to a lesser extent – upon TPR depletion, reflecting the known role of TPR and nuclear pore complexes in chromatin organisation at the nuclear periphery (38,39).

We next assessed the effect of NTF2 depletion on the heterochromatin mark H3K9me3 in control and HGPS fibroblasts. We observed a marked decrease in H3K9me3 staining intensity upon NTF2 depletion in control fibroblasts (Fig. 2C, D), similar to the basal H3K9me3 staining observed in HGPS cells expressing a control siRNA. NTF2 depletion did not further reduce H3K9me3 in HGPS cells. Moreover, we observed a similar decrease in H3K9me3 in high-passage-number (P61) unaffected human fibroblasts, suggesting that the perturbation observed in HGPS cells resembles what happens when unaffected cells reach senescence. In addition to the effect on chromatin, disrupting nuclear Ran by depleting NTF2

8

also promoted the entry of control fibroblasts into senescence as measured by senescence-associated β-galactosidase staining (Fig. 2E, F). However, depleting NTF2 in HGPS cells, which already had reduced nuclear Ran, did not significantly further increase the proportion of senescent cells. Collectively, these results suggested that the reduction in nuclear Ran observed in HGPS cells might, by globally affecting nucleocytoplasmic transport, contribute to downstream phenotypes of chromatin disorganisation and premature entry into senescence.

NAT10 inhibition reverses TNPO1 nuclear import pathway defects in HGPS cells

Neither the abundance nor the subcellular localisation of NTF2 appeared to be affected in HGPS cells (Fig. S3A), implying that defects in the Ran nuclear import machinery were not the cause of reduced nuclear accumulation of Ran in HGPS cells. Because NUP153 disruption reduces the nuclear abundance of Ran (20), we hypothesized that Ran gradient deregulation occurring in HGPS might reflect the loss of NUP153 nuclear import. This led us to investigate which upstream pathway(s) could affect NUP153 nuclear import in HGPS cells. NUP153 can be imported by several proteins, but evidence suggests that NUP153 is imported into the nucleus of interphase cells by the non-classic nuclear transport receptor TNPO1 (24), a karyopherin β protein that promotes nuclear import of only a specific subset of proteins, including NUP153 and hnRNPA1. We therefore assessed TNPO1 subcellular localization in control and HGPS fibroblasts by immunofluorescence staining. Whereas TNPO-1 was nearly equally distributed between the cytoplasm and nucleus in unaffected fibroblasts, TNPO1 was depleted from the nucleus in HGPS cells (Fig. 3 A-B), similarly to what we had observed for Ran (Fig. 1). To determine whether changes in the nuclear-to-cytoplasmic ratio of TNPO1 in HGPS cells had an impact on its nuclear importer function, we assessed the subcellular localization of hnRNPA1, one of the best-described TNPO1 cargo proteins. In accord with TNPO1 pathway deficiency in HGPS cells, we observed a

marked decrease of nuclear hnRNPA1 in these cells (Fig. 3A). Similar defects were observed

for the Ewing sarcoma protein (EWS), another characterised TNPO1 cargo (40) (Fig. S3B,

C). In contrast, the localization of NAT10, the subcellular distribution of which is not

detectably affected in HGPS (Fig. S4A and as described in (21)), was not altered upon

interfering with TNPO1 function by expressing MBP-M9M, a peptide that binds to TNPO1

and competes with its natural substrates (41) (Fig. S4B). These results identify the TNPO1

nuclear import pathway as deregulated in HGPS.

We also observed loss of nuclear TNPO1 in cells from unaffected aged individuals (Fig. 3C),

with no apparent change in the abundance of TNPO1 or hnRNPA1, similarly to HGPS cells

(Fig. 3D). Because NAT10 inhibition normalized NUP153 and TPR nuclear accumulation

and nuclear Ran abundance in HGPS cells (Fig. 1), we the effects of NAT10 inhibition on the

TNPO1 pathway. Both Remodelin treatment and siRNA-mediated NAT10 depletion restored

the nuclear-to-cytoplasmic ratio of TNPO1 in HGPS cells so that it was comparable to that of

control fibroblasts (Fig. 3 A-B). Taken together, these results suggested that the TNPO1

pathway is affected in both HGPS cells and in cells from aged individuals, leading to defects

in the nuclear import of TNPO1 and its cargos, including hnRNPA1 and NUP153, thereby

contributing to downstream defects of the RanGTP gradient. We conclude that NAT10

inhibition results in global normalisation of TNPO1 subcellular localisation and function in

HGPS cells, thereby alleviating downstream phenotypes. Although TNPO1 depletion itself

reduced proliferation of normal retinal pigmented epithelial RPE-1 cells (Fig. S5A), the

TNPO1 pathway defects observed in HGPS and in ageing cells did not appear to be a mere

consequence of slower cell growth. Indeed, mimicking reduced cell growth through serum

starvation of RPE-1 cells and control fibroblasts did not discernibly affect the TNPO1

pathway, nor the subcellular localisation of Ran or H3K9me3 (Fig. S5B-D), all of which are strongly affected in HGPS cells.

Modulation of microtubule stability by NAT10 inhibition affects the TNPO1 pathway

We previously observed that HGPS fibroblasts have a more stable microtubule network than control cells (21) and that this contributes to HGPS cellular phenotypes. We also showed that NAT10 inhibition improved these phenotypes, at least in part by targeting and destabilizing microtubules, thus releasing cytoskeletal forces on the nucleus and normalizing nuclear shape (21). This is in accord with a pool of NAT10 being associated with the cytoskeleton, as observed by subcellular fractionation and immunofluorescence (Fig. S6A-B). To assess whether there was a link between accumulation of TNPO1 in the cytoplasm of HGPS cells and microtubule stability, we first performed a PLA assay between TNPO1 and α-tubulin. Despite similar TNPO1 and α-tubulin staining intensities observed by immunofluorescence (Fig. S7A) and similar protein abundance observed by Western blotting (Fig. S7B), the interaction between TNPO1 and α-tubulin was significantly greater in HGPS fibroblasts than in control fibroblasts, whether measured per cell or per defined area of cytoplasm (Fig. 4A-B). The reason for measuring the number of PLA spots within a defined area was to account for the fact that senescent cells are larger than non-senescent cells, which could have biased the results. However, there was a significant increase in the number of PLA spots even within a defined area of cytoplasm (Fig. 4B right panel), showing that the increased interaction was not a reflection of the increased size of HGPS cells. The interaction between TNPO1 and α-tubulin was confirmed by immunoprecipitation using extracts of control fibroblasts (Fig. S7C).

To understand whether the effect of NAT10 inhibition on TNPO1 was associated with microtubule stabilization, we treated unaffected and HGPS fibroblasts with the microtubule stabilizing or destabilizing agents tubacin or nocodazole, respectively (Fig. 4C). Mimicking microtubule stabilization, such as occurs in HGPS cells, by treating control fibroblasts with tubacin led to significant defects in both TNPO1 and hnRNPA1 nuclear import (Fig. 4C-D). By contrast, destabilizing microtubules in HGPS cells or in cells from unaffected aged individuals with nocodazole enhanced TNPO1 nuclear localization and, presumably by promoting TNPO1 transport function, increased the nuclear abundance of hnRNPA1 (Fig. 4C-D and Fig. S8). These results suggested that the TNPO1 import pathway can be altered by microtubule stability, and that by modulating this, NAT10 inhibition re-balanced the TNPO1 nuclear-to-cytoplasm ratio and enhanced the nuclear import of TNPO1 cargo proteins.

Normalisation of HGPS cells by NAT10 inhibition requires TNPO1

To determine whether the normalization of heterochromatin markers and decreased senescence that we previously observed in HGPS cells upon NAT10 inhibition (21) depended on TNPO1, we treated control and HGPS fibroblasts with siRNAs to deplete NAT10 alone or in combination with NUP153 or TNPO1 depletion. As we observed previously (20), NUP153 depletion in control cells led to loss of nuclear Ran, probably because it affects the structure of nuclear pore complexes that are important for RanGTP gradient formation. However, NUP153 depletion did not affect the TNPO1 pathway, as observed by the normal subcellular localisation of TNPO1 and its downstream target hnRNPA1 (Fig. S9). Cells impaired in nuclear Ran due to TNPO1 depletion (Fig. 5A and Fig. S10) or as observed in HGPS cells (Fig. 5B), also displayed significantly reduced abundance of the heterochromatin marker H3K9me3 (Fig. 5C). This is in accordance with the chromatin decompaction that we observed upon Ran deregulation (Fig. 2B, C) and suggested that TNPO1 depletion was

12

sufficient to cause this phenotype. Furthermore, simultaneous depletion of NUP153 and

NAT10 in control fibroblasts produced similar H3K9me3 phenotypes compared to NUP153

depletion alone (Fig. 5A, C), identifying NUP153 as a critical mediator of NAT10-dependent

cellular rebalancing. Whereas NAT10 depletion alone restored nuclear Ran and H3K9me3

staining in HGPS cells, this did not happen when NUP153 or TNPO1 was co-depleted with

NAT10 (Fig. 5B, C). Similarly, although NAT10 depletion strongly decreased the proportion

of HGPS cells positive for senescence-associated β-galactosidase, this was not the case when

NUP153 or TNPO1 was co-depleted with NAT10 (Fig. 5D-E). These results indicated that

the normalization of phenotypes caused by NAT10 depletion in HGPS cells indeed occurred

through restoration of TNPO1 pathway function. Thus, when TNPO1 or its cargo NUP153 is

absent, NAT10-dependent phenotypic rescue does not occur. TNPO1 or NUP153 depletion in

control fibroblasts also promoted senescence, implying that the TNPO1 pathway is important

for maintaining cellular homeostasis.

TNPO1 is required for NAT10 inhibition-mediated gene expression modulation

In light of the above observations, we hypothesized that enhancing TNPO1-mediated nuclear

import in HGPS cells by inhibiting NAT10 might have an impact on gene expression. To test

this idea, we performed global gene expression analysis on HGPS fibroblasts compared to

control fibroblasts, both after 8 weeks of DMSO-only or Remodelin treatment (media was

supplemented with fresh Remodelin every 3 days). Volcano plots of each individual

differential expression analysis (Fig. 6A) show log10-adjusted p-values plotted against log2

fold gene expression changes. Significant genes (based on a fold-change threshold of 2-fold

up or down and an adjusted p-value threshold of 0.05) are indicated by the red (increased

expression) and blue (decreased expression) regions of the plots. As expected and as

previously reported (32,36,42), we observed deregulation of gene expression in HGPS cells

compared to control fibroblasts (Fig. 6A left panel and Fig. 6B row 1), with 137 and 221 genes showing significantly increased or decreased expression, respectively. Notably, chronic long-term treatment with Remodelin had very little effect on gene expression in control fibroblasts, with only 17 genes exhibiting significantly increased or decreased expression (Fig. 6A). In marked contrast, Remodelin had a strong effect on HGPS cells (Fig. 6A), modifying the expression of 652 genes (Table S1). Strikingly, these Remodelin-induced gene expression changes in HGPS cells were largely reciprocal to the gene expression differences between HGPS cells and unaffected cells (Fig. 6B). Thus, long-term Remodelin treatment had a strong rebalancing effect on the expression of most genes that are deregulated in HGPS cells.

Next, we asked whether the gene expression changes mediated by NAT10 inhibition would still occur in the absence of TNPO1. To address this question, we performed a separate microarray analysis following short-term depletion of NAT10, TNPO1, or both NAT10 and TNPO1 by siRNA. We used NAT10 siRNA instead of Remodelin in this experiment to enable rigorous comparison to siRNA-mediated depletion of TNPO1. Due to the shorter timeframe of siRNA experiments, we applied a lower threshold (1.5-fold up or down) in this analysis, which increased the number of deregulated genes in HGPS cells treated with a control siRNA (Fig. 6C) compared to earlier experiments with Remodelin (Fig. 6A). Similar to Remodelin treatment, NAT10 depletion modified the expression of more genes in HGPS cells than it did in control fibroblasts (Fig. 6C and Table S2) and had a stronger effect than Remodelin on control fibroblasts. Indeed, siRNA-mediated NAT10 depletion abolished all functions of NAT10, such as its RNA helicase activity and its role in ribosome biogenesis (43). Even though we did observe a rebalancing effect on some HGPS deregulated genes (Fig. 6D), short-term NAT10 depletion by siRNA treatment did not have comparable effects

to Remodelin treatment on global gene expression rebalancing (Fig. 6D). This suggests that long-term NAT10 inhibition is required to observe global rebalancing of the HGPS gene expression profile.

To assess whether gene expression changes mediated by NAT10 depletion were occurring through TNPO1, we compared NAT10 depletion alone with simultaneous depletion of NAT10 and TNPO1 (Fig. 7A). We observed that 70% of the genes showing significantly increased or decreased expression upon NAT10 depletion alone in control fibroblasts were not additionally modified upon simultaneous depletion of TNPO1 (Fig. 7B, Tables S3-4), despite similar NAT10 protein knock-down (Fig. 7A). In HGPS cells, this number was reduced to 40% (Fig. 7C), likely a result of the deregulation of additional pathways. However, because we observed that the TNPO1 pathway was required for the NAT10 inhibition–mediated phenotypic changes in HGPS cells, we hypothesized that this specific set of genes (Fig. 7C) would be mainly responsible for the HGPS cellular rescue. Gene ontology analysis of those genes significantly affected by NAT10 depletion only (Table S5) and not by simultaneous depletion of NAT10 and TNPO1 in HGPS cells showed an enrichment for various cellular components (Fig. 7D), including cell-substrate junctions and focal adhesions, extracellular matrix, and endoplasmic reticulum for genes showing decreased expression or Golgi and small ribosomal subunits for genes showing increased expression. When we plotted this specific set of genes that we refer to as "siNAT10 only" genes on a heatmap (Fig. 7E), we observed that the expression of about 40% of this specific set of genes was rebalanced towards the expression observed in control fibroblasts (Fig. 7E).

Finally, to assess whether the TNPO1 pathway was affected in HGPS, we compared the effect of TNPO1 depletion on gene expression profiles in control fibroblasts (Fig. 7F) with

15

gene expression in HGPS fibroblasts treated with a control siRNA compared to control

fibroblasts treated with a control siRNA (Fig. 7F). This showed that 58% of the genes

exhibiting significantly increased or decreased expression upon TNPO1 depletion in control

fibroblasts showed a similar trend in HGPS cells treated with control siRNA (Fig. 7F).

TNPO1 depletion can be expected to have differential effects compared to a change of

TNPO1 subcellular localisation as observed in HGPS, where the protein is still expressed but

is mislocalized (Fig. 7A and Fig. 7F). Moreover, short-term TNPO1 depletion by siRNA

might not recapitulate the effects of long-term decreased nuclear abundance of TNPO1

observed in HGPS cells. These results however support our hypothesis that the TNPO1

pathway is affected in HGPS and that NAT10 inhibition mediates gene expression changes,

at least in part through TNPO1. Collectively, our results suggest that NAT10 inhibition

enhances global HGPS cell fitness by restoring TNPO1 function, thus rebalancing nucleo-

cytoplasmic transport, which restores normal chromatin organization and control of gene

expression and prevents premature entry into senescence.

DISCUSSION

TNPO1 dysfunction in HGPS drives nuclear Ran defects

In this study, we established that the TNPO1 nuclear importer is mislocalized in cells derived from patients with HGPS. Furthermore, we found that defective nuclear import of TNPO1 cargo proteins including NUP153 (24) and hnRNPA1 (27) appeared to contribute to downstream phenotypic defects in HGPS cells, including abnormal nuclear pore assembly, chromatin disorganisation, gene expression changes, and premature entry into senescence. Although previous studies had reported RanGTP gradient defects in cells from HGPS patients (9,10), the mechanism behind it was still unclear. Given the known link between oxidative stress and nucleocytoplasmic transport (as reviewed in (44)), and because oxidative stress is higher in HGPS cells (11), it was thought to be the main cause of decreased nuclear Ran abundance in progeria. However, oxidative stress has been shown to affect classical importin-mediated nuclear import pathways (45), whereas we found here that the TNPO1 pathway appeared to be most affected in HGPS. Therefore, based on our findings herein, we suggest that depletion of Ran from the nucleus in HGPS cells is a consequence of dysfunctional TNPO1, rather than a direct effect of the presence of progerin, oxidative stress, or NUP153 deregulation. In addition, by showing that NAT10 inhibition restores TNPO1-dependent nuclear import by releasing TNPO1 from the cytoplasm of HGPS cells, we have provided insights into how NAT10 inhibition, through its effects on microtubule stability, ameliorates cellular defects of HGPS cells. As described previously (21), NAT10 inhibition does not affect progerin abundance or localisation, suggesting that its effects on HGPS cells occur through a progerin-independent pathway.

It is still unclear how NAT10 activity might increase during normal and premature ageing. However, it has been suggested that NAT10 activity is modulated by auto-acetylation and that sirtuin proteins can mediate NAT10 deacetylation (46). Sirtuin proteins have been linked to various age-related pathologies (reviewed in (47)), with their decreased activity being associated with senescence. In this context, reactivation of SIRT1 has been shown to extend health and lifespan in an HGPS mouse model (48). Therefore, we speculate that decreased sirtuin activity as occurs in aging might lead to increased NAT10 acetylation and activity, therefore contributing to increased microtubule stability and retention of TNPO1 in the cytoplasm. Whether the acetylation of other reported NAT10 substrates such as p53 (49), the upstream binding factor (UBF) (50), and rRNA (51) is also affected in HGPS warrants investigation.

Microtubule stability modulates nucleocytoplasmic transport

Based on our findings, we propose a model for how TNPO1-mediated nuclear import affects the nucleocytoplasmic RanGTP gradient and how sequestration of TNPO1 in the cytoplasm perturbs this process (Fig. 8). **1)** Under normal circumstances, TNPO1 binds to specific cargo proteins, such as NUP153, in the cytoplasm. **2)** The TNPO1-cargo complex is translocated into the nucleus through the nuclear pore, which is anchored to microtubules and microfilaments in the cytoplasm (52). **3)** Once in the nucleus and upon RanGTP binding to TNPO1, the NUP153 cargo dissociates from TNPO1 and is incorporated as a component of the NPC basket structure, which is responsible for anchoring TPR (18,19), the last nucleoporin to be assembled on the NPC (53). The resulting mature NPC is then fully functional for nucleocytoplasmic transport and other NPC-dependent roles, such as anchoring chromatin. **4)** During the progression of HGPS and during ageing of unaffected cells, increased microtubule network stability appears to sequester TNPO1 and its cargo proteins in

the cytoplasm. **5)** As a consequence, TNPO1 cargoes, like NUP153, are not imported properly into the nucleus, which prevents NUP153 from being incorporated efficiently into NPCs. This in turn affects the nuclear import of Ran, resulting in decreased nuclear Ran abundance, as well as defects of TPR anchorage at NPCs. Consequently, during the progression of HGPS and upon normal-cell ageing, there is progressive chromatin disorganisation and decompaction, global gene expression changes, and premature entry into senescence. We speculate that the global dysregulation of gene expression observed in HGPS cells is probably a consequence of both a direct effect of abnormal nuclear architecture on chromatin organisation and of nucleocytoplasmic transport defects affecting the nuclear import of various proteins, including TPR, which directly binds chromatin (39) and hnRNPA1, which modulates the activity of transcription factors (28-30). **6)** By destabilising the microtubule network (21), NAT10 inhibition releases TNPO1 from the cytoplasm in HGPS or in cells from unaffected aged individuals, thus enhancing its nuclear translocation together with the ensuing nuclear import of its cargos such as NUP153 and hnRNPA1. This then substantially normalizes chromatin organisation, Ran-mediated nucleocytoplasmic transport, and global transcription patterns. In support of this model, wherein NAT10 inhibition ameliorates HGPS phenotypes through the TNPO1 pathway, we found that Remodelin had little effect on HGPS phenotypes when the cells had been depleted of TNPO1.

In addition to helping to explain the mechanistic basis for HGPS cell dysfunction, our study highlights how specific components of the nucleocytoplasmic transport machinery are affected by a range of factors, in this case cytoskeletal integrity. This correlates with the finding that mechanical forces can modulate nuclear pore opening and conformation, thereby modifying nucleocytoplasmic transport efficiency (54). Finally, our study underscores the

potential for NAT10 inhibition as a possible therapeutic strategy for HGPS, and perhaps also for certain pathologies associated with aging.

MATERIAL AND METHODS

Cell culture and transfections

Control skin primary fibroblasts from a young healthy individual (GM03440, 20 years old), from two Hutchinson-Gilford progeria syndrome patients (AG11498: 14 years old and AG11513: 8 years old), and from four aged individuals (AG11240: 81 years old female, AG04059: 96 years old male, AG05248: 87 years old male, AG09602: 92 years old female) were purchased from Coriell Cell Repositories and used in passage-matched cells (unless indicated otherwise on the figure) between passage numbers 9 and 25. Cells were grown in Dulbecco's modified Eagle medium (DMEM, Sigma-Aldrich) supplemented with 10% fetal bovine serum (BioSera), 2mM L-glutamine, 100U per ml penicillin, 100 μg ml^{-1} streptomycin. Normal Retinal Pigmented Epithelial Cells (RPE-1) were grown in DMEM:F12 (Sigma-Aldrich) supplemented with 10% fetal bovine serum (BioSera), 2mM L-glutamine, 100U per ml penicillin, 100 μg ml^{-1} streptomycin. For serum starvation experiments, the same medium was used without any fetal bovine serum. The following siRNA duplexes were purchased from Life Sciences: NAT10 stealth RNAi: GAGCAUGGACCUCUCUGAAUACAUA, and stealth RNAi negative control duplexes. TNPO1 siRNAs were from Sigma Aldrich: GCAAAGAUGUACUCGUAAG, GUAUAGAGAUGCAGCCUUA, and GUAAAUACCAGCAUAAGAA. Smart pool NUP153 and NTF2 siRNA oligonucleotides where purchased from Dharmacon. siRNA transfections were carried out using Lipofectamine RNAiMax (Life Sciences), following the manufacturer's instructions. Cells were analysed 48 to 72 h after transfection. U2OS human osteosarcoma cells were grown in DMEM supplemented as above. A plasmid encoding the TNPO1 inhibitor Myc-MBP-M9M (41) was transfected using Lipofectamine 2000 (Life Sciences), following the manufacturer's instructions. Cells were analysed 24h after transfection.

Cell proliferation

Non-transformed human RPE-1 cells were plated at equivalent low densities and transfected with control (siCT) or TNPO1 (siTNPO1) siRNA as explained above. Six days later, cells were fixed and stained with crystal violet staining solution (0.5% Crystal Violet, 20% methanol).

Cell growth inhibition

RPE-1 cells or control fibroblasts were kept in either normal medium supplemented with 10% fetal bovine serum (FBS) or in medium without serum to arrest cell proliferation. After 4 days of serum deprivation, cells were processed for immunofluorescence.

Drug treatments

Remodelin was synthetized as described previously (21) and added to cell cultures for a final concentration of 1 μM for at least 5 days, replacing the medium every 3 days. For immunofluorescence assays, Nocodazole and Tubacin were added to the medium for 16h at 100ng/ml and 10μM, respectively.

Senescence assay

Senescence was assessed 72h after siRNA transfection using the Senescence β-Galactosidase Staining Kit #9860 from Cell Signaling Technology. Blue cells were counted using the Cell Counter plugin from Image J.

Immunoblotting

Total cell extracts were prepared by scraping cells from culture plates in SDS lysis buffer (4% SDS, 20% glycerol, and 120 mM Tris-HCl, pH 6.8), boiling for 5 min at 95°C, followed by 10 strokes through a 25-gauge needle. Before loading, lysates were diluted with a solution of 0.01% bromophenol blue and 200 mM DTT and boiled for 5 min at 95°C. Proteins were resolved by SDS-PAGE on 4-12% gradient gels (NUPAGE, Life Sciences) and transferred onto nitrocellulose membrane (Protran; Whatman). Secondary antibodies conjugated to IRDye 800CW were from LI-COR Biosciences and used at 1:10000. Detection was performed with an imager (Odyssey; LI-COR Biosciences).

Subcellular fractionation

Cells were harvested with trypsin-EDTA and centrifuged at 500xg for 5 min. Cells were washed once with 1ml ice-cold PBS and centrifuged at 500xg for 5min. Supernatant was removed, and 20μl of packed cell volume was processed for subcellular fractionation using the kit for cultured cells from ThermoFisher (Cat number 78840), using the manufacturer's instructions. Subcellular fractions were then processed for immunoblotting as described above. Protein compartmentalisation in chromatin and cytoskeletal fractions was assessed by detection of the Histone H3 and alpha-Tubulin proteins.

Immunofluorescence

Cells were washed with PBS and fixed for 20 min with 2% PFA in PBS. Cells were permeabilised for 5 min with PBS/0.2% Triton X-100, and blocked with PBS/0.2% Tween 20 (PBS-T) containing 5% BSA. Coverslips were incubated for 1 h with primary antibodies and for 30 min with appropriate secondary antibodies coupled to Alexa Fluor 488, 594 or 647 fluorophores (Life Technologies, 1:1000), before being incubated with 2μg/ml DAPI. Pictures were acquired with a FluoView 1000 confocal microscope (Olympus) using the

same laser power for matching images and antibodies. All the immunofluorescence experiments were performed at least 3 times independently and the pictures shown in the figures are representative images of the 3 experiments. Image analyses were carried out with the Volocity software (PerkinElmer) using the following protocol: Find objects (DAPI). Subpopulation: Fill holes in objects. Exclude touching edge of image. Exclude objects by size: $<100\mu m^2$. Measure. The fluorescence intensity in each channel was then recorded.

Proximity Ligation Assay (PLA)

The PLA assays were carried out using the Duolink® In Situ Red Starter Kit Mouse/Rabbit (DUO9101, Sigma Aldrich) following manufacturer's instructions. Image analysis was carried out with the Volocity software (PerkinElmer) using the following protocol: Find objects (DAPI). Exclude objects $>1000\mu m^2$ and $<20\mu m^2$. Fill holes in objects. Exclude touching edge of image. Find spots using intensity. Compartmentalize: Divide spots – Between nuclei. Select ROI and record the number of PLA spots.

Primary Antibodies

All of the antibodies used in this study and the concentrations at which they were used for immunofluorescence and Western blotting are summarized in Table S6.

Micrococcal nuclease digestion sensitivity assay

Because this assay requires a lot of cells, we could not perform it with HGPS cells and thus used human osteosarcoma U2OS cells instead. $1x10^6$ cells were trypsinized, harvested, and washed once with 1ml of 1xRSB buffer (10 mM Tris, pH 7.6, 15 mM NaCl, and 1.5 mM $MgCl_2$). After centrifugation (300 x g), the cell pellet was resuspended in 1 ml of 1x RSB buffer with 1% Triton-X 100 and homogenized by five strokes with a loose-fitting glass

pestle to release nuclei. Nuclei were collected by centrifugation (13, 000 x g) and washed twice with 1 ml of buffer A (15 mM Tris, pH 7.5, 15 mM NaCl, 60 mM KCl, 0.34 M sucrose, 0.5 mM spermidine, 0.15 mM spermine, 0.25 mM PMSF, and 0.1% β-mercaptoethanol). Nuclei were resuspended in Buffer A and aliquoted into 100 μl aliquots. 1.2μl of 0.1 M CaCl2 was added to each aliquot and nuclei were digested by addition of 0.25 μl of 200 U/ml MNase (Sigma-Aldrich) and incubated at 30°C. Each aliquot was put back on ice at different time points and digestion was immediately stopped by addition of 3μl EDTA. DNA was purified using the Qiagen PCR purification kit and 1500 ng of DNA was analysed on a 1.5% agarose gel. Digestion profiles were analysed using ImageJ and values were adjusted relative to the global intensity of each lane to compensate for DNA loading variations.

Microarray analysis

Long-term Remodelin treatment for microarray experiments was performed by keeping and passaging cells in medium containing 1 μM Remodelin or DMSO only for 12 population doublings. Three independent biological replicates were used for each condition. RNA extracted from cells was purified using Direct-zol RNA MiniPrep kit (Zymo Research, cat. no. R2072) and treated with DNaseI (Zymo), according to manufacturers' instructions. RNA quality was assessed using the Tapestation (Agilent Technologies) and Qubit (Invitrogen). Quality analysis of total RNA, hybridisation and data capture was performed at the Cambridge Genomic Services. Illumina HumanHT-12 v4 beadchips were used for gene expression screening. Results were analysed using the *Lumi* (55) Bioconductor package in R. Probe-level data were combined to give gene-level data by taking the mean of all probes for a single gene. Differentially expressed genes were identified in each cell line using *limma* (56), using a 2-way factorial design with disease state as the first factor (HGPS vs control fibroblasts) and treatment as the second factor (Remodelin vs DMSO, or

siNAT10/siTNPO1/both vs siCT). Differentially expressed genes were calculated by performing pairwise comparisons between the four groups (Treated Normal, Untreated Normal, Treated HGPS, Untreated HGPS) for each treatment. All resulting p-values were corrected for multiple testing by using the Benjamini and Hochberg False Discovery Rate correction (52). Genes were defined as showing significantly altered expression if they showed a fold change greater than some threshold value (2-fold up or down for Remodelin, 1.5-fold up or down for siRNA) compared to control, with an adjusted p-value lower than 0.05.

SUPPLEMENTARY MATERIALS

Fig. S1. NAT10 inhibition rescues impaired TPR nuclear localisation in cells from aged individuals.

Fig. S2. Nuclear import is affected in HGPS.

Fig. S3. TNPO1-dependent protein cargos are affected in HGPS cells.

Fig. S4. NAT10 nuclear import does not depend on TNPO1.

Fig. S5. Cell proliferation inhibition does not affect the Transportin-1 pathway.

Fig. S6. NAT10 localises both in the nucleus and in the cytoskeleton.

Fig. S7. TNPO1 accumulates at the microtubule network of HGPS cells.

Fig. S8. Microtubule destabilization rescues TNPO1 pathway defects in HGPS cells and in cells from aged individuals**.**

Fig. S9. NUP153 depletion does not affect the Transportin-1 pathway.

Fig. S10. Efficiency of protein depletions.

Table S1. List of genes modified by Remodelin treatment.

Table S2. List of genes modified by NAT10 depletion.

Table S3. List of genes modified by depletion of TNPO1 and NAT10.

Table S4. List of genes modified by TNPO1 depletion.

Table S5. Gene ontology analysis of "siNAT10-only" genes.

Table S6. Primary antibodies.

REFERENCES AND NOTES

1. De Sandre-Giovannoli, A., Bernard, R., Cau, P., Navarro, C., Amiel, J., Boccaccio, I., Lyonnet, S., Stewart, C. L., Munnich, A., Le Merrer, M., and Levy, N. (2003) Lamin a truncation in Hutchinson-Gilford progeria. *Science* **300**, 2055

2. Eriksson, M., Brown, W. T., Gordon, L. B., Glynn, M. W., Singer, J., Scott, L., Erdos, M. R., Robbins, C. M., Moses, T. Y., Berglund, P., Dutra, A., Pak, E., Durkin, S., Csoka, A. B., Boehnke, M., Glover, T. W., and Collins, F. S. (2003) Recurrent de novo point mutations in lamin A cause Hutchinson-Gilford progeria syndrome. *Nature* **423**, 293-298

3. Goldman, R. D., Gruenbaum, Y., Moir, R. D., Shumaker, D. K., and Spann, T. P. (2002) Nuclear lamins: building blocks of nuclear architecture. *Genes Dev* **16**, 533-547

4. Liu, B., Wang, J., Chan, K. M., Tjia, W. M., Deng, W., Guan, X., Huang, J. D., Li, K. M., Chau, P. Y., Chen, D. J., Pei, D., Pendas, A. M., Cadinanos, J., Lopez-Otin, C., Tse, H. F., Hutchison, C., Chen, J., Cao, Y., Cheah, K. S., Tryggvason, K., and Zhou, Z. (2005) Genomic instability in laminopathy-based premature aging. *Nat Med* **11**, 780-785

5. Scaffidi, P., and Misteli, T. (2005) Reversal of the cellular phenotype in the premature aging disease Hutchinson-Gilford progeria syndrome. *Nat Med* **11**, 440-445

6. Lopez-Otin, C., Blasco, M. A., Partridge, L., Serrano, M., and Kroemer, G. (2013) The hallmarks of aging. *Cell* **153**, 1194-1217

7. Gordon, L. B., Massaro, J., D'Agostino, R. B., Sr., Campbell, S. E., Brazier, J., Brown, W. T., Kleinman, M. E., Kieran, M. W., and Progeria Clinical Trials, C. (2014) Impact of farnesylation inhibitors on survival in Hutchinson-Gilford progeria syndrome. *Circulation* **130**, 27-34

8.   Merideth, M. A., Gordon, L. B., Clauss, S., Sachdev, V., Smith, A. C., Perry, M. B., Brewer, C. C., Zalewski, C., Kim, H. J., Solomon, B., Brooks, B. P., Gerber, L. H., Turner, M. L., Domingo, D. L., Hart, T. C., Graf, J., Reynolds, J. C., Gropman, A., Yanovski, J. A., Gerhard-Herman, M., Collins, F. S., Nabel, E. G., Cannon, R. O., 3rd, Gahl, W. A., and Introne, W. J. (2008) Phenotype and course of Hutchinson-Gilford progeria syndrome. *N Engl J Med* **358**, 592-604

9.   Kelley, J. B., Datta, S., Snow, C. J., Chatterjee, M., Ni, L., Spencer, A., Yang, C. S., Cubenas-Potts, C., Matunis, M. J., and Paschal, B. M. (2011) The defective nuclear lamina in Hutchinson-gilford progeria syndrome disrupts the nucleocytoplasmic Ran gradient and inhibits nuclear localization of Ubc9. *Mol Cell Biol* **31**, 3378-3395

10.   Snow, C. J., Dar, A., Dutta, A., Kehlenbach, R. H., and Paschal, B. M. (2013) Defective nuclear import of Tpr in Progeria reflects the Ran sensitivity of large cargo transport. *J Cell Biol* **201**, 541-557

11.   Datta, S., Snow, C. J., and Paschal, B. M. (2014) A pathway linking oxidative stress and the Ran GTPase system in progeria. *Mol Biol Cell* **25**, 1202-1215

12.   Gorlich, D., Pante, N., Kutay, U., Aebi, U., and Bischoff, F. R. (1996) Identification of different roles for RanGDP and RanGTP in nuclear protein import. *Embo J* **15**, 5584-5594

13.   Bischoff, F. R., Klebe, C., Kretschmer, J., Wittinghofer, A., and Ponstingl, H. (1994) RanGAP1 induces GTPase activity of nuclear Ras-related Ran. *Proc Natl Acad Sci U S A* **91**, 2587-2591

14.   Bischoff, F. R., and Ponstingl, H. (1991) Catalysis of guanine nucleotide exchange on Ran by the mitotic regulator RCC1. *Nature* **354**, 80-82

15.   Klebe, C., Bischoff, F. R., Ponstingl, H., and Wittinghofer, A. (1995) Interaction of the nuclear GTP-binding protein Ran with its regulatory proteins RCC1 and RanGAP1. *Biochemistry* **34**, 639-647

16.   Hetzer, M., Gruss, O. J., and Mattaj, I. W. (2002) The Ran GTPase as a marker of chromosome position in spindle formation and nuclear envelope assembly. *Nat Cell Biol* **4**, E177-184

17.   Izaurralde, E., Kutay, U., von Kobbe, C., Mattaj, I. W., and Gorlich, D. (1997) The asymmetric distribution of the constituents of the Ran system is essential for transport into and out of the nucleus. *Embo J* **16**, 6535-6547

18.   Hase, M. E., and Cordes, V. C. (2003) Direct interaction with nup153 mediates binding of Tpr to the periphery of the nuclear pore complex. *Mol Biol Cell* **14**, 1923-1940

19.   Krull, S., Thyberg, J., Bjorkroth, B., Rackwitz, H. R., and Cordes, V. C. (2004) Nucleoporins as components of the nuclear pore complex core structure and Tpr as the architectural element of the nuclear basket. *Mol Biol Cell* **15**, 4261-4277

20.   Cobb, A. M., Larrieu, D., Warren, D. T., Liu, Y., Srivastava, S., Smith, A. J., Bowater, R. P., Jackson, S. P., and Shanahan, C. M. (2016) Prelamin A impairs 53BP1 nuclear entry by mislocalizing NUP153 and disrupting the Ran gradient. *Aging Cell*

21.   Larrieu, D., Britton, S., Demir, M., Rodriguez, R., and Jackson, S. P. (2014) Chemical inhibition of NAT10 corrects defects of laminopathic cells. *Science* **344**, 527-532

22.   Lau, C. K., Delmar, V. A., Chan, R. C., Phung, Q., Bernis, C., Fichtman, B., Rasala, B. A., and Forbes, D. J. (2009) Transportin regulates major mitotic assembly events: from spindle to nuclear pore assembly. *Mol Biol Cell* **20**, 4043-4058

23.   Shah, S., Tugendreich, S., and Forbes, D. (1998) Major binding sites for the nuclear import receptor are the internal nucleoporin Nup153 and the adjacent nuclear filament protein Tpr. *J Cell Biol* **141**, 31-49

24. Vollmer, B., Lorenz, M., Moreno-Andres, D., Bodenhofer, M., De Magistris, P., Astrinidis, S. A., Schooley, A., Flotenmeyer, M., Leptihn, S., and Antonin, W. (2015) Nup153 Recruits the Nup107-160 Complex to the Inner Nuclear Membrane for Interphasic Nuclear Pore Complex Assembly. *Dev Cell* **33**, 717-728

25. Pollard, V. W., Michael, W. M., Nakielny, S., Siomi, M. C., Wang, F., and Dreyfuss, G. (1996) A novel receptor-mediated nuclear protein import pathway. *Cell* **86**, 985-994

26. Siomi, M. C., Eder, P. S., Kataoka, N., Wan, L., Liu, Q., and Dreyfuss, G. (1997) Transportin-mediated nuclear import of heterogeneous nuclear RNP proteins. *J Cell Biol* **138**, 1181-1192

27. Fridell, R. A., Truant, R., Thorne, L., Benson, R. E., and Cullen, B. R. (1997) Nuclear import of hnRNP A1 is mediated by a novel cellular cofactor related to karyopherin-beta. *J Cell Sci* **110 (Pt 11)**, 1325-1331

28. Dreyfuss, G., Matunis, M. J., Pinol-Roma, S., and Burd, C. G. (1993) hnRNP proteins and the biogenesis of mRNA. *Annu Rev Biochem* **62**, 289-321

29. Huelga, S. C., Vu, A. Q., Arnold, J. D., Liang, T. Y., Liu, P. P., Yan, B. Y., Donohue, J. P., Shiue, L., Hoon, S., Brenner, S., Ares, M., Jr., and Yeo, G. W. (2012) Integrative genome-wide analysis reveals cooperative regulation of alternative splicing by hnRNP proteins. *Cell Rep* **1**, 167-178

30. Jean-Philippe, J., Paz, S., and Caputi, M. (2013) hnRNP A1: the Swiss army knife of gene expression. *Int J Mol Sci* **14**, 18999-19024

31. Moore, M. S. (1998) Ran and nuclear transport. *J Biol Chem* **273**, 22857-22860

32. Aliper, A. M., Csoka, A. B., Buzdin, A., Jetka, T., Roumiantsev, S., Moskalev, A., and Zhavoronkov, A. (2015) Signaling pathway activation drift during aging: Hutchinson-Gilford Progeria Syndrome fibroblasts are comparable to normal middle-age and old-age cells. *Aging (Albany NY)* **7**, 26-37

33. Fredriksson, S., Gullberg, M., Jarvius, J., Olsson, C., Pietras, K., Gustafsdottir, S. M., Ostman, A., and Landegren, U. (2002) Protein detection using proximity-dependent DNA ligation assays. *Nature biotechnology* **20**, 473-477

34. Smith, A., Brownawell, A., and Macara, I. G. (1998) Nuclear import of Ran is mediated by the transport factor NTF2. *Curr Biol* **8**, 1403-1406

35. Ribbeck, K., Lipowsky, G., Kent, H. M., Stewart, M., and Gorlich, D. (1998) NTF2 mediates nuclear import of Ran. *Embo J* **17**, 6587-6598

36. Csoka, A. B., English, S. B., Simkevich, C. P., Ginzinger, D. G., Butte, A. J., Schatten, G. P., Rothman, F. G., and Sedivy, J. M. (2004) Genome-scale expression profiling of Hutchinson-Gilford progeria syndrome reveals widespread transcriptional misregulation leading to mesodermal/mesenchymal defects and accelerated atherosclerosis. *Aging Cell* **3**, 235-243

37. Goldman, R. D., Shumaker, D. K., Erdos, M. R., Eriksson, M., Goldman, A. E., Gordon, L. B., Gruenbaum, Y., Khuon, S., Mendez, M., Varga, R., and Collins, F. S. (2004) Accumulation of mutant lamin A causes progressive changes in nuclear architecture in Hutchinson-Gilford progeria syndrome. *Proc Natl Acad Sci U S A* **101**, 8963-8968

38. Krull, S., Dorries, J., Boysen, B., Reidenbach, S., Magnius, L., Norder, H., Thyberg, J., and Cordes, V. C. (2010) Protein Tpr is required for establishing nuclear pore-associated zones of heterochromatin exclusion. *Embo J* **29**, 1659-1673

39. Vaquerizas, J. M., Suyama, R., Kind, J., Miura, K., Luscombe, N. M., and Akhtar, A. (2010) Nuclear pore proteins nup153 and megator define transcriptionally active regions in the Drosophila genome. *PLoS Genet* **6**, e1000846

40. Guttinger, S., Muhlhausser, P., Koller-Eichhorn, R., Brennecke, J., and Kutay, U. (2004) Transportin2 functions as importin and mediates nuclear import of HuR. *Proc Natl Acad Sci U S A* **101**, 2918-2923

41.   Cansizoglu, A. E., Lee, B. J., Zhang, Z. C., Fontoura, B. M., and Chook, Y. M. (2007) Structure-based design of a pathway-specific nuclear import inhibitor. *Nat Struct Mol Biol* **14**, 452-454

42.   Marji, J., O'Donoghue, S. I., McClintock, D., Satagopam, V. P., Schneider, R., Ratner, D., Worman, H. J., Gordon, L. B., and Djabali, K. (2010) Defective lamin A-Rb signaling in Hutchinson-Gilford Progeria Syndrome and reversal by farnesyltransferase inhibition. *PLoS One* **5**, e11132

43.   Ito, S., Horikawa, S., Suzuki, T., Kawauchi, H., Tanaka, Y., Suzuki, T., and Suzuki, T. (2014) Human NAT10 is an ATP-dependent RNA acetyltransferase responsible for N4-acetylcytidine formation in 18 S ribosomal RNA (rRNA). *J Biol Chem* **289**, 35724-35730

44.   Kodiha, M., and Stochaj, U. (2012) Nuclear transport: a switch for the oxidative stress-signaling circuit? *J Signal Transduct* **2012**, 208650

45.   Kodiha, M., Chu, A., Matusiewicz, N., and Stochaj, U. (2004) Multiple mechanisms promote the inhibition of classical nuclear import upon exposure to severe oxidative stress. *Cell Death Differ* **11**, 862-874

46.   Cai, S., Liu, X., Zhang, C., Xing, B., and Du, X. (2017) Autoacetylation of NAT10 is critical for its function in rRNA transcription activation. *Biochem Biophys Res Commun* **483**, 624-629

47.   Giblin, W., Skinner, M. E., and Lombard, D. B. (2014) Sirtuins: guardians of mammalian healthspan. *Trends Genet* **30**, 271-286

48.   Liu, B., Ghosh, S., Yang, X., Zheng, H., Liu, X., Wang, Z., Jin, G., Zheng, B., Kennedy, B. K., Suh, Y., Kaeberlein, M., Tryggvason, K., and Zhou, Z. (2012) Resveratrol rescues SIRT1-dependent adult stem cell decline and alleviates progeroid features in laminopathy-based progeria. *Cell Metab* **16**, 738-750

49. Liu, X., Tan, Y., Zhang, C., Zhang, Y., Zhang, L., Ren, P., Deng, H., Luo, J., Ke, Y., and Du, X. (2016) NAT10 regulates p53 activation through acetylating p53 at K120 and ubiquitinating Mdm2. *EMBO Rep* **17**, 349-366

50. Kong, R., Zhang, L., Hu, L., Peng, Q., Han, W., Du, X., and Ke, Y. (2011) hALP, a novel transcriptional U three protein (t-UTP), activates RNA polymerase I transcription by binding and acetylating the upstream binding factor (UBF). *J Biol Chem* **286**, 7139-7148

51. Sharma, S., Langhendries, J. L., Watzinger, P., Kotter, P., Entian, K. D., and Lafontaine, D. L. (2015) Yeast Kre33 and human NAT10 are conserved 18S rRNA cytosine acetyltransferases that modify tRNAs assisted by the adaptor Tan1/THUMPD1. *Nucleic acids research* **43**, 2242-2258

52. Joseph, J., and Dasso, M. (2008) The nucleoporin Nup358 associates with and regulates interphase microtubules. *FEBS Lett* **582**, 190-196

53. Bodoor, K., Shaikh, S., Salina, D., Raharjo, W. H., Bastos, R., Lohka, M., and Burke, B. (1999) Sequential recruitment of NPC proteins to the nuclear periphery at the end of mitosis. *J Cell Sci* **112 (Pt 13)**, 2253-2264

54. Elosegui-Artola, A., Andreu, I., Beedle, A. E. M., Lezamiz, A., Uroz, M., Kosmalska, A. J., Oria, R., Kechagia, J. Z., Rico-Lastres, P., Le Roux, A. L., Shanahan, C. M., Trepat, X., Navajas, D., Garcia-Manyes, S., and Roca-Cusachs, P. (2017) Force Triggers YAP Nuclear Entry by Regulating Transport across Nuclear Pores. *Cell* **171**, 1397-1410 e1314

55. Du, P., Kibbe, W. A., and Lin, S. M. (2008) lumi: a pipeline for processing Illumina microarray. *Bioinformatics* **24**, 1547-1548

56. Ritchie, M. E., Phipson, B., Wu, D., Hu, Y., Law, C. W., Shi, W., and Smyth, G. K. (2015) limma powers differential expression analyses for RNA-sequencing and microarray studies. *Nucleic acids research* **43**, e47

Author contributions: DL designed, carried out and analysed all experiments, except the microarray and wrote the paper. EV carried out the microarray experiment and commented on the manuscript. SR analysed all microarray data, generated the corresponding graphs and legends. SB helped with revisions of the paper by repeating western blots. SPJ supervised the study and helped writing and editing the manuscript. TK commented on the manuscript. **Competing interests:** DL and SPJ are named inventors on a patent WO 2015/150824 describing compounds that include Remodelin and their use in premature ageing syndromes and other laminopathies. SPJ is a member of the scientific advisory board of Carrick Therapeutics, and DL and SPJ have received consulting fees over the past 3 years from Carrick Therapeutics, which is engaged in activities related to the subject matter of this study. The other authors declare that they have no competing interests. **Data and materials availability:** The small molecule Remodelin used in this study

was synthesized by Dr Raphael Rodriguez (Curie Institute, Paris) and obtained under an

MTA through the Centre National de la Recherche Scientifique (CNRS). The raw data and

processed differential expression tables from the microarray are available from ArrayExpress

under accession number E-MTAB-6651 (https://www.ebi.ac.uk/arrayexpress/experiments/E-

MTAB-6651/).
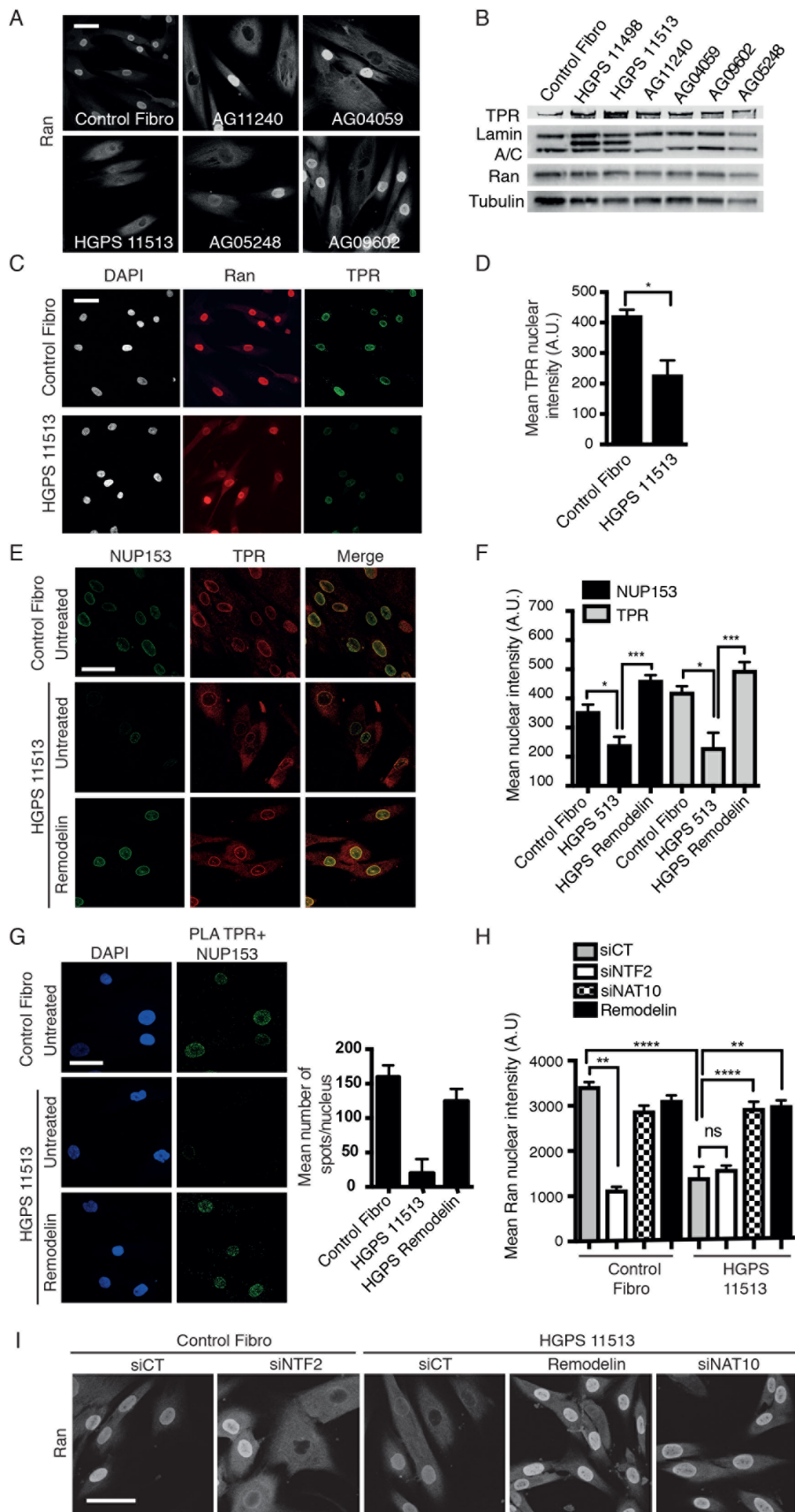
Fig. 1 NAT10 inhibition rescues the reduced nucleocytoplasmic transport in progeric and aged cells. (**A**) Representative immunofluorescence images showing subcellular localisation of Ran in skin fibroblasts from a 20-year-old healthy male (Control fibro), aged individuals (AG11240, a 81-year-old female; AG04059, a 96-year-old male; AG05248, a 87-year old-male; AG09602, a 92-year-old female), and an 8-year-old HGPS patient (HGPS 11513). N = 3 independent experiments. (**B**) Representative Western blot showing the abundance of the indicated proteins in extracts of fibroblasts from young, aged, and HGPS individuals. N = 3 independent experiments. (**C**) Representative immunofluorescence images showing nuclear Ran and TPR in HGPS cells as compared to control cells. (**D**) Quantification of TPR nuclear intensity in the indicated cells. N = 3 independent experiments, n>100 nuclei per experiment for each cell type. *p=0.016 (Mann Whitney test). Error bars indicate s.e.m. (**E**) Representative immunofluorescence images showing localization of NUP153 and TPR in control and HGPS fibroblasts in the absence (untreated) or presence of the NAT10 inhibitor Remodelin. (**F**) Quantification of NUP153 and TPR nuclear intensity from experiments in (E). N = 3 independent experiments, n>70 nuclei per experiment for each cell type. P values from left to right: *p=0.0111, ***p=0.0002, *p=0.0163, ***p=0.0007 (Mann Whitney test). Error bars indicate s.e.m. (**G**) Proximity ligation assay (PLA) showing the interaction of TPR and NUP153 in control and HGPS fibroblasts in the absence (untreated) or presence of the NAT10 inhibitor Remodelin. Results of the PLA were quantified as the mean number of dots per nucleus. N = 3 independent experiments, n>50 nuclei per experiment for each cell type. (**H**) and (**I**) Ran nuclear localisation in control and HGPS fibroblasts upon siRNA-mediated depletion of NTF2 (siNTF2) or NAT10 (siNAT10) or upon NAT10 inhibition (Remodelin). siCT, control siRNA. N = 3 independent experiments, n>70 nuclei per experiment for each cell type. P values from left to right: **p=0.0043, ****p<0.0001, ns: non significant,

****p<0.0001, **p=0.0029 (Mann Whitney test). Error bars indicate s.e.m. All scale bars, 50μm.

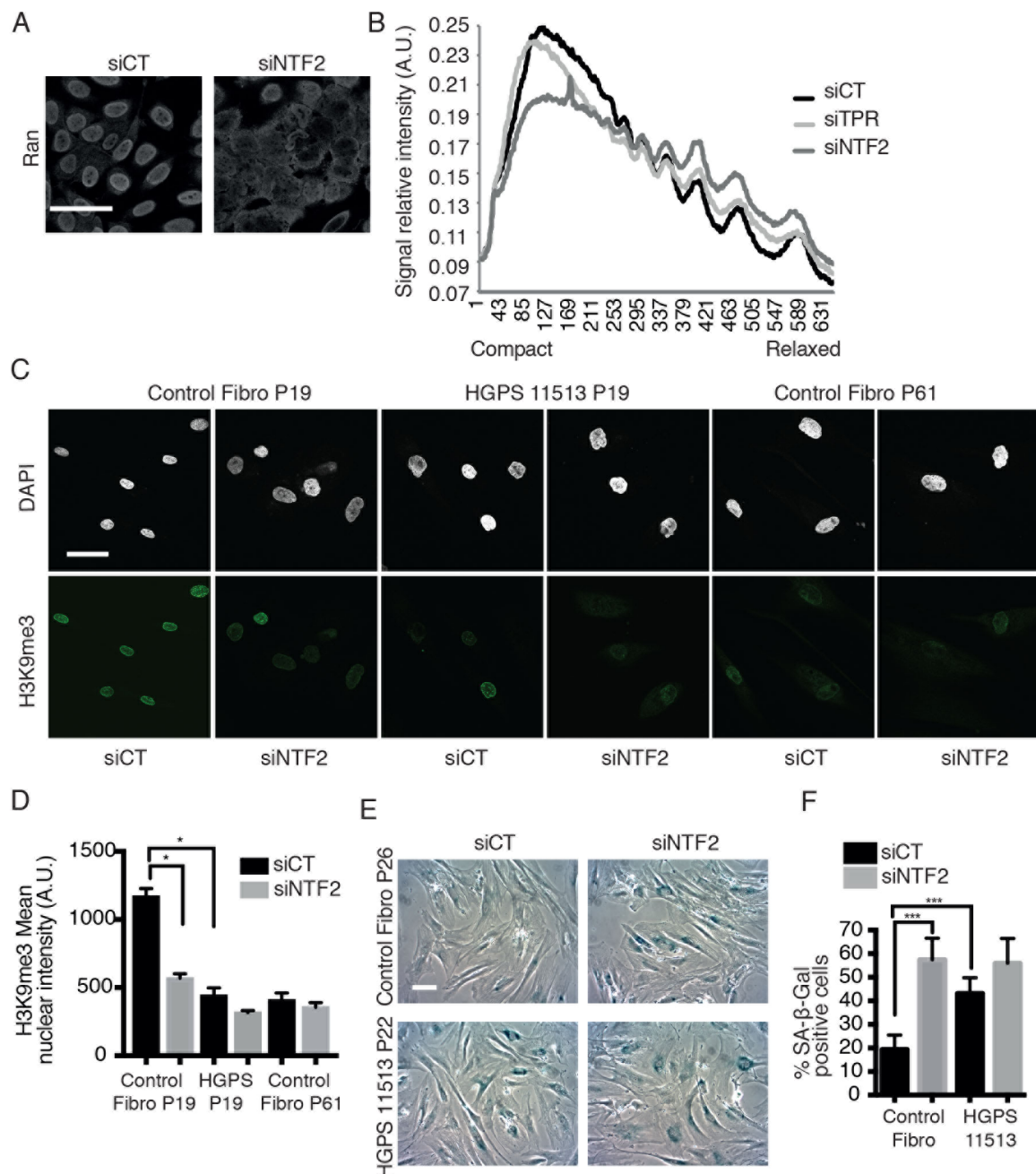**Fig. 2 Disruption of Ran induces chromatin relaxation and senescence.** (**A** and **B**) Analysis of chromatin relaxation by MNase assay in U2OS cells upon siRNA-mediated TPR depletion (siTPR) or disruption of Ran nuclear import by NTF2 depletion (siNTF2). siCT,

control siRNA. Scale bar, 30μm. Digested chromatin was analysed on an agarose gel and quantified using ImageJ. The graph is a representative figure of three independent experiments and represents the relative bands intensity (y axis) of the digested nucleosomes that migrate further from the well (x axis) because the chromatin is more relaxed, and thus more accessible to the MNase enzyme. (**C**) Representative immunofluorescence images showing H3K9me3 staining in young fibroblasts at passage number 19 (Control Fibro P19), old fibroblasts at passage number 61 (Control Fibro P61), and HGPS cells at passage 19 (HGPS 11513 P19) upon transfection with siCT or siNTF2 to disrupt the RanGTP gradient. Scale bar, 50μm. (**D**) Quantification of H3K9me3 nuclear intensity from (C). N = 2 independent experiments, n>50 nuclei per experiment for each cell type. P values from left to right: *p=0.0159, *p=0.014 (Mann Whitney test). Error bars indicate s.e.m. (**E**) Senescence-associated β-galactosidase staining (blue cells) upon transfection with siCT or siNTF2 siRNA in control (Control fibro) and HGPS (HGPS 11513) fibroblasts at the indicated passage number (P). Scale bar, 50μm. (**F**) Quantification of blue cells from experiments in (C). N = 3 independent experiments, n>200 nuclei per experiment for each cell type. P values from left to right: ***p=0.0003, ***p=0.0002 (Mann-Whitney test). Error bars indicate s.e.m.
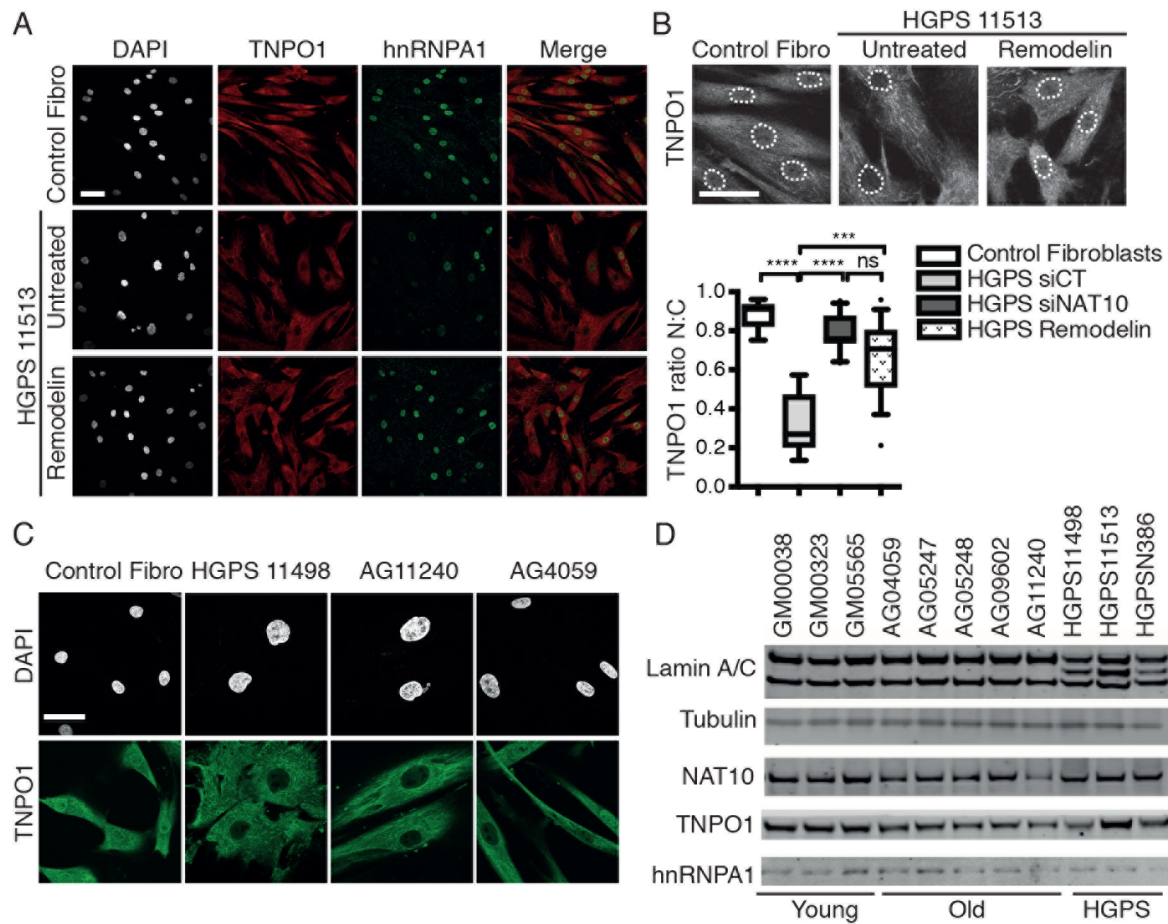
Fig. 3 The TNPO1 pathway is defective in HGPS cells and rescued by NAT10 inhibition.
(**A**) Representative immunofluorescence images showing the subcellular localization of
TNPO1 and its cargo hnRNPA1 in control and HGPS fibroblasts in the absence (untreated)
or presence of the NAT10 inhibitor Remodelin. (**B**) Higher magnification images from panel
(A) showing TNPO1 nuclear and cytoplasmic subcellular localisation, quantified below as
nuclear-to-cytoplasmic ratio (N:C). Nuclei are outlined with white dotted lines. Box plots
represent median (line), 10-90 percentiles (whiskers) and outliers (dots). N = 3 independent
experiments, n>50 nuclei per experiment for each cell type. P values from left to right:
****$p<0.0001$, ***$p=0.0003$, ****$p<0.0001$, ns: non significant. (Mann Whitney test). Error
bars indicate s.e.m. (**C**). Representative immunofluorescence images showing TNPO1
subcellular localisation in fibroblasts from other HGPS patients (HGPS 11498) and in cells

from healthy aged individuals (AG11240 and AG059). N = 3 independent experiments. (**D**) Western blot showing total TNPO1 and hnRNPA1 abundance in the indicated cells. N = 3 independent experiments. All scale bars, 50μm.
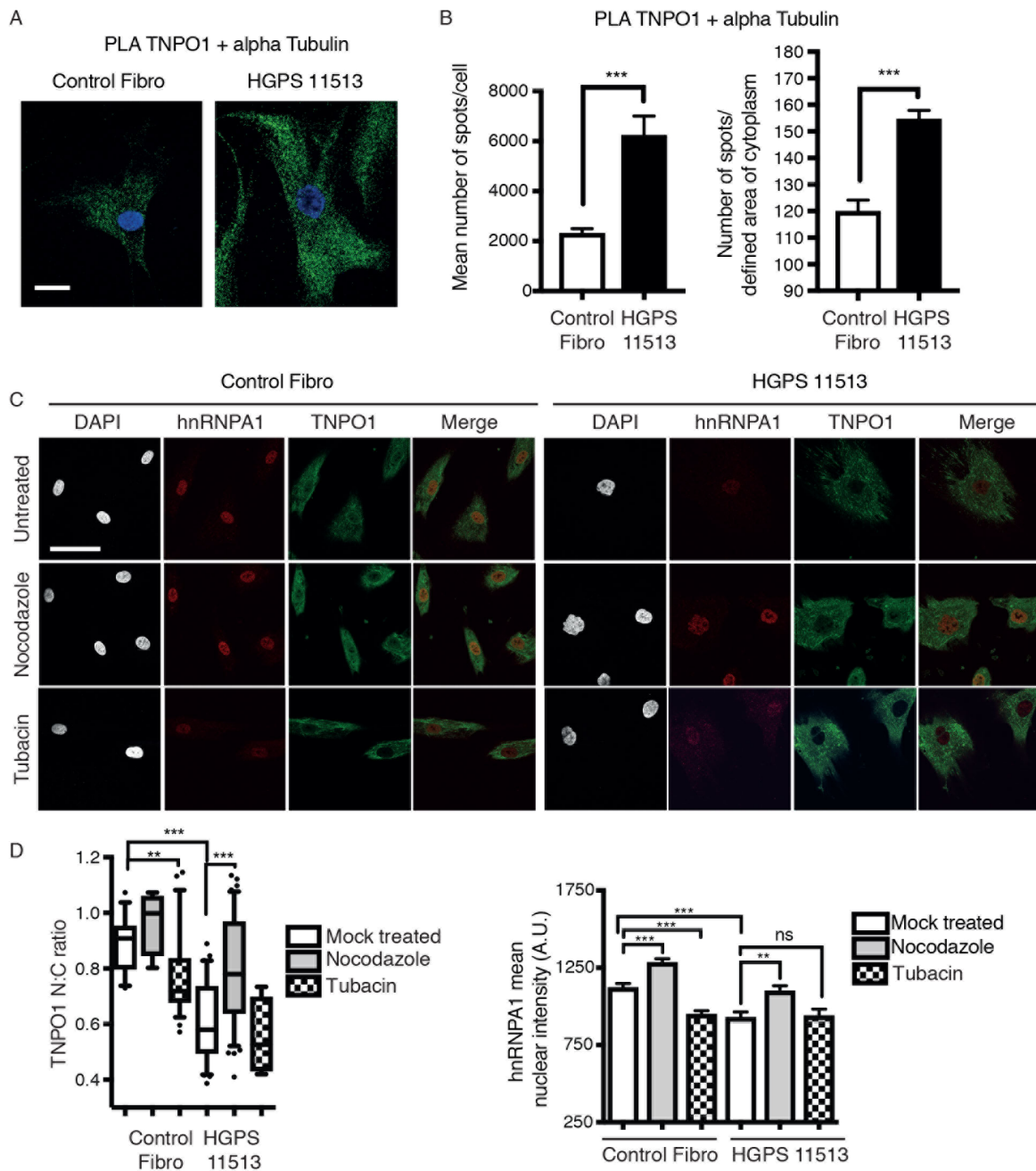
Fig. 4 Microtubule reorganisation modulates TNPO1 localisation and function. (A)
Representative immunofluorescence images from proximity ligation assays (PLA) in control
and HGPS fibroblasts using antibodies recognizing TNPO1 and α-tubulin. Each dot
represents an interaction between one molecule of TNPO1 and one molecule of alpha-
tubulin. Scale bar, 20μm. **(B)** Quantification of the PLA assays shown in (A), representing

both the total number of dots per cell (left) or the average number of spots in a defined area of cytoplasm (right). N = 3 independent experiments, n>46 nuclei per experiment for each cell type. P values: ***p=0.0005, ***p=0.0003 (Mann Whitney test). Error bars represent s.e.m. (**C**) Representative immunofluorescence images showing the effect of compounds that destabilize (nocodazole) or stabilize (tubacin) the microtubule network on the nuclear localization of TNPO1 and its cargo hnRNPA1. Scale bar, 50μm. (**D**) Quantification of the TNPO1 nuclear-to-cytoplasmic ratio (N:C) and of hnRNPA1 nuclear intensity. Box plots represent median (line), 10-90 percentiles (whiskers) and outliers (dots). N = 3 independent experiments, n>50 nuclei per experiment for each cell type. Top graph p values from left to right: **p=0.0011, ***p=0.0002, ***p=0.0002, ns: non significant. Bottom graph p values from left to right: ***p=0.0002, ***p=0.0001, ***p=0.0001, **p=0.0023, ns: non significant (Mann Whitney test). Error bars represent s.e.m.
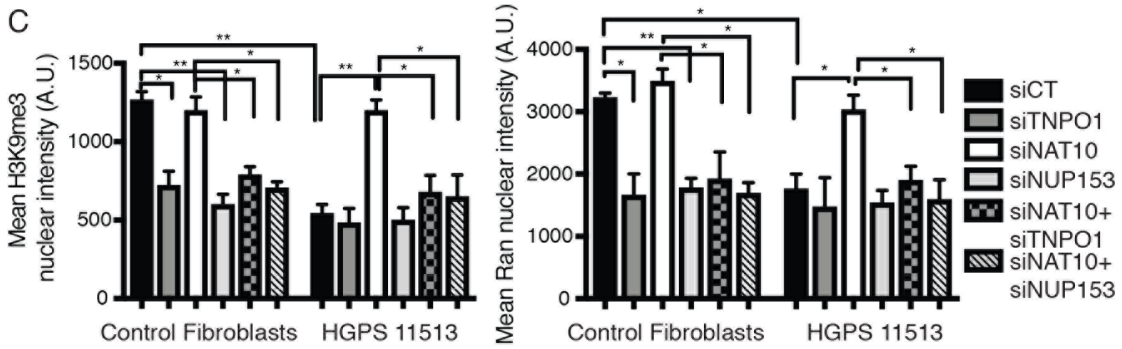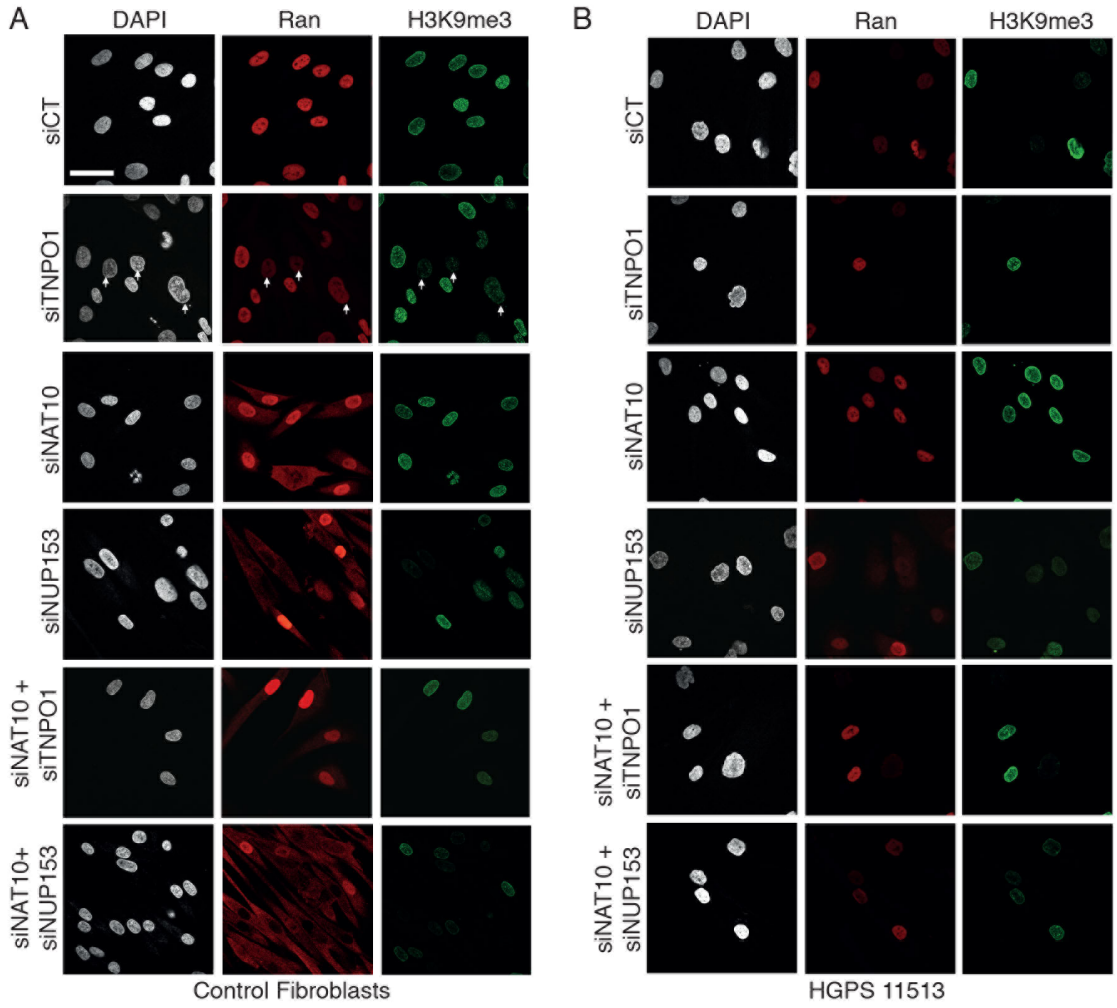
A Control Fibroblasts

DAPI | Ran | H3K9me3

siCT / siTNPO1 / siNAT10 / siNUP153 / siNAT10 + siTNPO1 / siNAT10+ siNUP153

B HGPS 11513

DAPI | Ran | H3K9me3

siCT / siTNPO1 / siNAT10 / siNUP153 / siNAT10 + siTNPO1 / siNAT10 + siNUP153

C

Mean H3K9me3 nuclear intensity (A.U.) — Control Fibroblasts / HGPS 11513

Mean Ran nuclear intensity (A.U.) — Control Fibroblasts / HGPS 11513

siCT
siTNPO1
siNAT10
siNUP153
siNAT10+ siTNPO1
siNAT10+ siNUP153

D HGPS 11513

siCT | siNAT10 | siTNPO1 | siNAT10+siTNPO1

E

% SA-β-Gal positive cells — Control Fibroblasts / HGPS 11513

siCT
siTNPO1
siNAT10
siNUP153
siNAT10+ siTNPO1

46

Fig. 5 TNPO1 is required for cellular normalisation mediated by NAT10 inhibition. (A and B) Representative immunofluorescence images showing Ran and H3K9me3 staining in control (A) or HGPS (B) fibroblasts after transfection with the indicated siRNA. (See Fig. S10 for protein knockdown efficiency). N = 3 independent experiments. Scale bar, 50μm. (**C**) Quantification of H3K9me3 and Ran nuclear intensity from the cells in (A) and (B). N = 3 independent experiments, n>150 cells per experiment for each cell type. P values from left to right: H3K9me3 in control fibroblasts: *p=0.0195, **p=0.0087, *p=0.0315, *p=0.0197, **p=0.0064. H3K9me3 in HGPS fibroblasts: **p=0.0097, *p=0.03, *p=0.0393. Ran in control fibroblasts: *p=0.025, **p=0.0075, *p=0.0443, *p=0.011, *p=0.015. Ran in HGPS fibroblasts: *p=0.0342, *p=0.0407, *p=0.0368 (Unpaired t test). Error bars indicate s.e.m. (**D**) Senescence-associated β-galactosidase (SA-β-Gal) staining in HGPS fibroblasts that had been treated with the indicated siRNAs. (**E**) Quantification of SA-β-Gal staining in (D). N = 3 independent experiments, n>200 cells per experiment for each cell type. P values from left to right: *p=0.0107, *p=0.049, ***p=0.0001, ****p<0.0001, ns: non significant (Unpaired t test). Error bars indicate s.e.m.
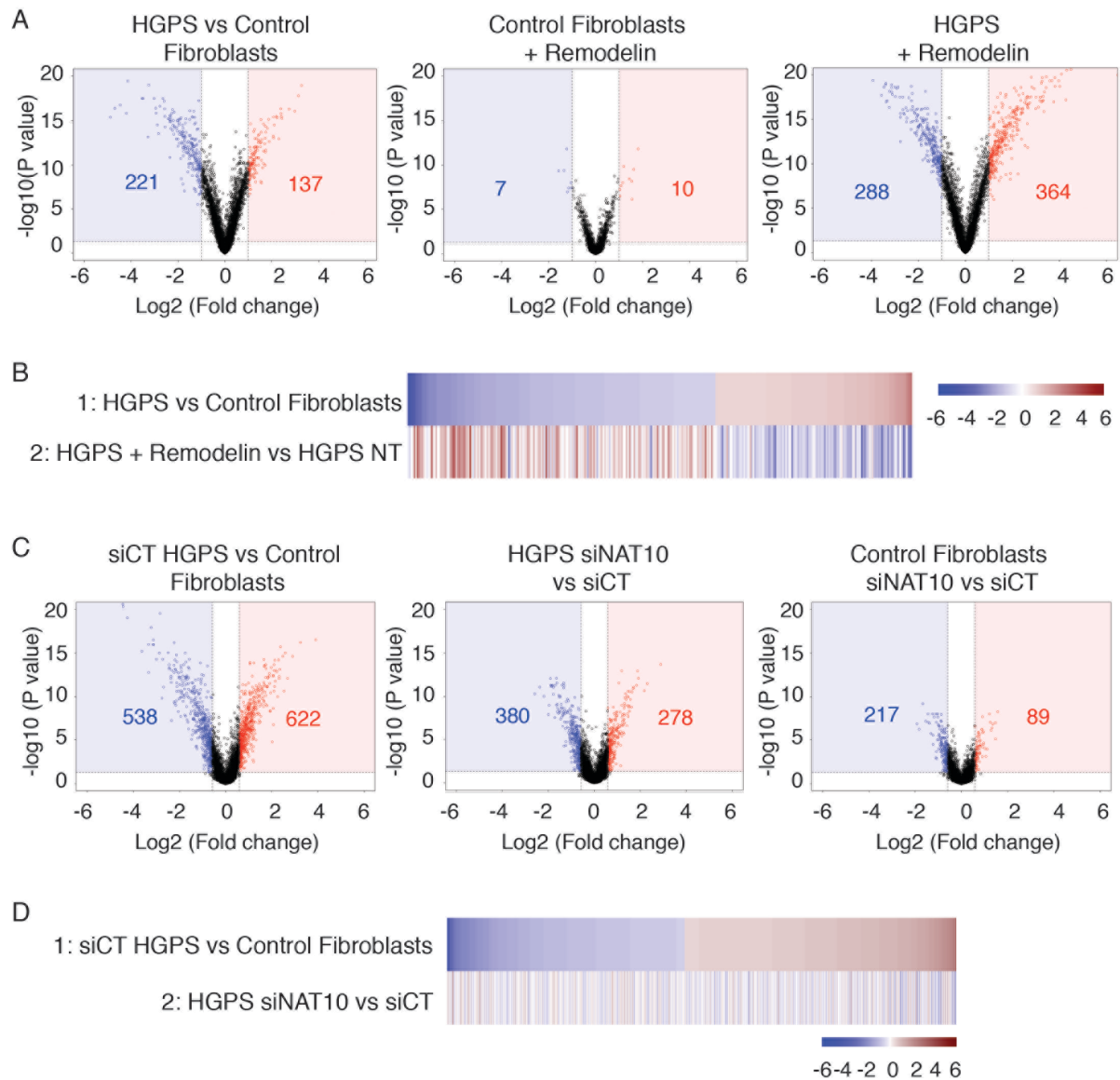
Fig. 6 Effects of NAT10 inhibition or depletion on gene expression. (**A**) Volcano plots from the microarray analysis showing the number of genes with decreased (blue) or increased (red) expression in HGPS fibroblasts compared to control fibroblasts, in control fibroblasts treated with Remodelin, and in HGPS fibroblasts treated with Remodelin. N = 3 independent experiments. The log10 of the adjusted p-value is used such that the more significant a gene in gene expression is, the higher it will appear on the y-axis. The log2 of the fold change is used such that genes with increased (red) or decreased (blue) expression have equal weighting in the plot. Genes were classified as showing gene expression changes if they

showed a change of 2-fold (up or down) or greater with an adjusted p value less than or equal to 0.05. For both control and HGPS fibroblasts, Remodelin was used as a chronic treatment for eight weeks (middle and right panels). (**B**) Heat maps of genes with significantly altered expression from (A) showing the effect of Remodelin treatment on gene expression in HGPS cells. (**C**) Volcano plots from the microarray analysis showing the number of genes for which expression was decreased (blue) or increased (red) by 1.5-fold or greater under the indicated conditions. siRNA-mediated NAT10 depletion (siNAT10) and control siRNA treatment (siCT) was transient (5 days). N = 3 independent experiments. (**D**) Heat maps of genes presented with significantly altered expression from (C) showing the effect of NAT10 depletion on gene expression in HGPS cells.
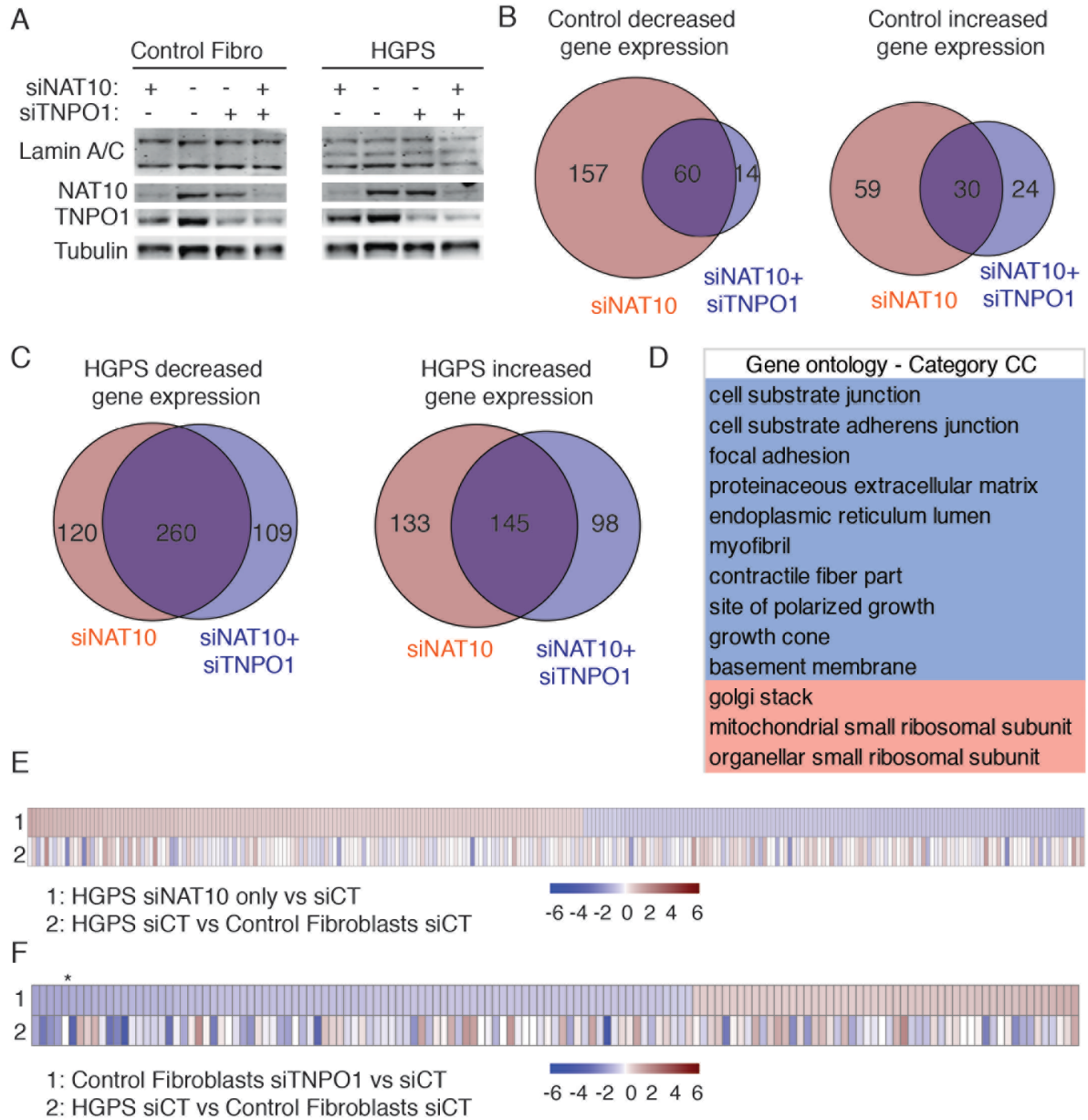
Fig. 7 NAT10 modulates gene expression through TNPO1. (**A**) Representative Western blotting analysis showing the efficiency of siRNA-mediated depletion of NAT10 (siNAT10) and TNPO1 (siTNPO1). N = 2 independent experiments. (**B** and **C**) Venn diagrams generated from the microarray analysis showing the overlap between genes with significantly increased or decreased expression upon NAT10 depletion alone or together with TNPO1 depletion (siNAT10+siTNPO1) in control (B) and HGPS (C) fibroblasts. (**D**) Gene ontology analysis

showing cellular component (CC) terms enrichment from genes with significantly decreased (blue) or increased (red) expression only upon NAT10 depletion in HGPS cells. (**E**) Heat maps of siNAT10-specific genes presented in (C) and (D), showing the gene expression changes for genes modified by siNAT10 only (compared to siCT) in HGPS cells (row 1) and their expression in HGPS cells compared to control fibroblasts (row 2). (**F**) Heat maps of genes with expression significantly modified by TNPO1 depletion in control fibroblasts (row 1), and their expression in HGPS cells compared to control fibroblasts (row 2). TNPO1 is indicated by an asterisk. All analyses were performed using three biological replicates.
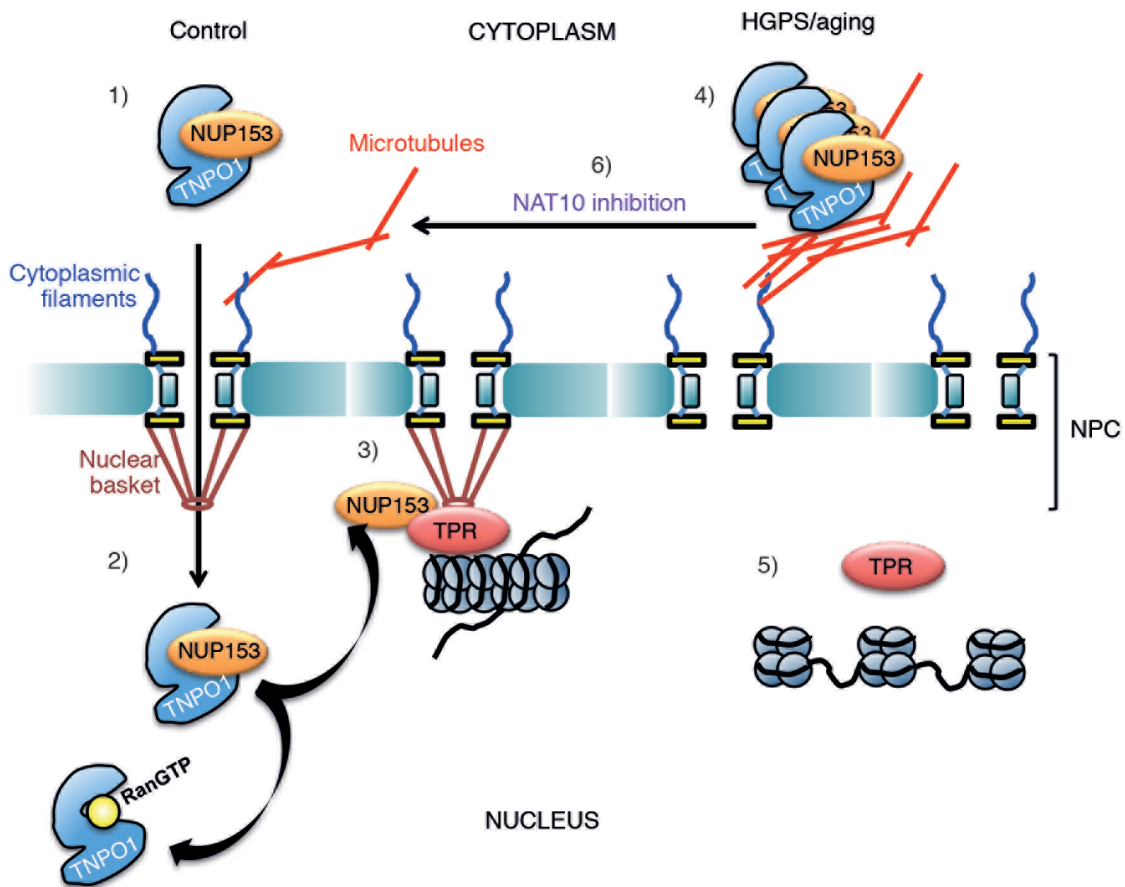
Fig. 8 Model for how NAT10 inhibition rescues HGPS phenotypes. 1) In control cells,

TNPO1 binds to its cargo proteins, such as NUP153, in the cytoplasm. **2)** The TNPO1-cargo

complex translocates into the nucleus through the nuclear pore. **3)** Once in the nucleus and

upon RanGTP binding to TNPO1, the NUP153 cargo dissociates from TNPO1 and is

incorporated into the nuclear pore complex (NPC) and recruits TPR to the NPC. Mature,

fully functional NPCs mediate nucleocytoplasmic transport and other roles, such as

anchoring chromatin to the nuclear envelope through TPR. **4)** In HGPS and aging, increased

microtubule network stability sequesters TNPO1 in the cytoplasm. **5)** TNPO1 cargos such as

NUP153 are not properly imported into the nucleus. The absence of NUP153 results in

decreased nuclear Ran abundance and defects in TPR anchorage at NPCs. This leads to

chromatin disorganisation, global gene expression changes, and premature entry into

senescence. **6)** By destabilising the microtubule network, NAT10 inhibition releases TNPO1 from the cytoplasm, enhancing its nuclear translocation together with nuclear import of its cargos such as NUP153 and hnRNPA1. This then substantially normalizes chromatin organisation, RanGTP mediated nucleocytoplasmic transport, and global transcription patterns.
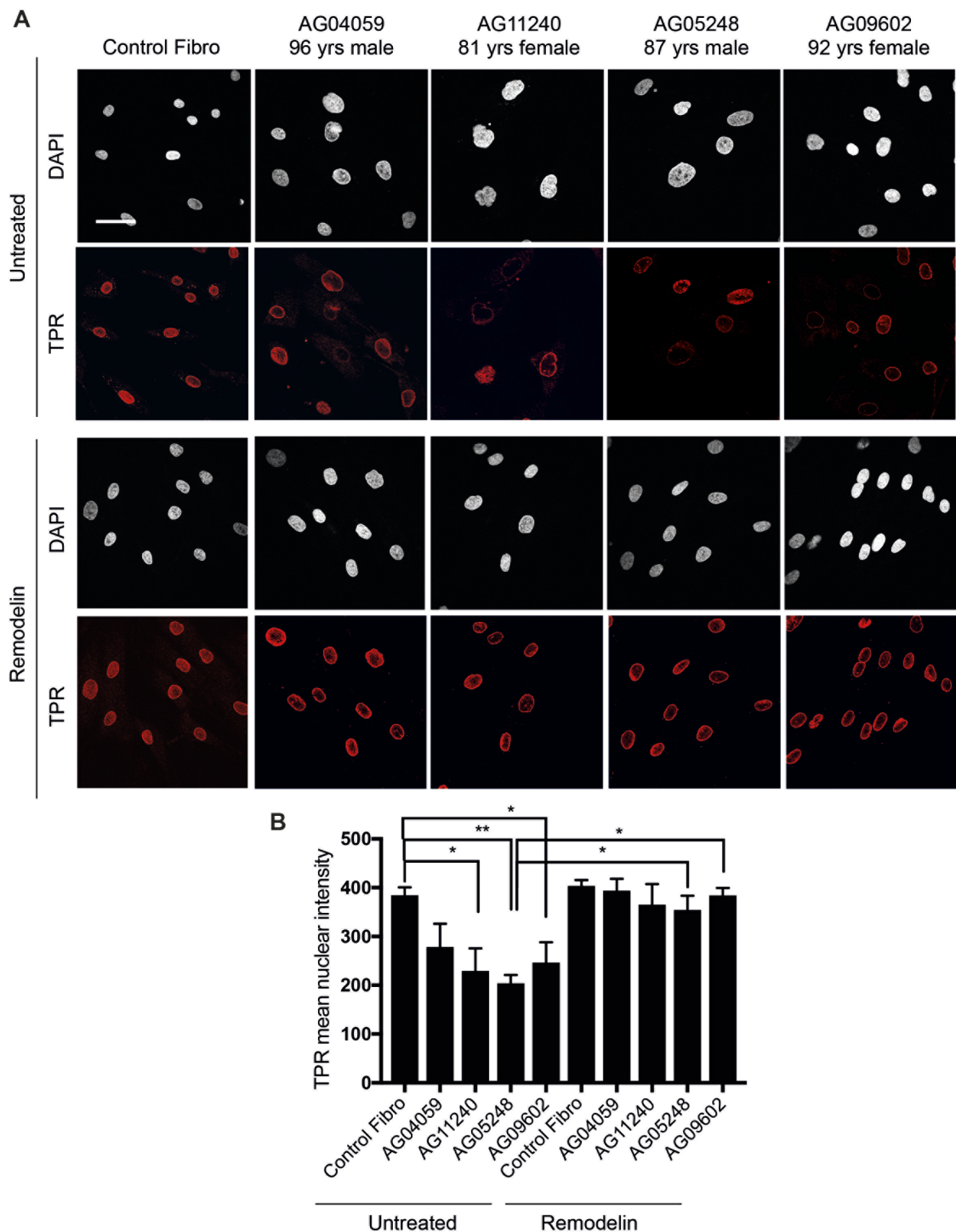
Fig. S1. TPR nuclear localisation is impaired in cells from aged individuals and normalised by NAT10 inhibition. (**A**) Representative immunofluorescence images from three independent experiments showing nuclear localization of TPR in the indicated cells in the absence (top) or presence (bottom) of Remodelin. Scale bar: 50μm. (**B**) Quantification of TPR nuclear intensity from three independent experiments as shown in **A** (Unpaired t test, error bars represent s.e.m. P values from left to right: *p=0.0462, **p=0.0086, *p=0.0485, *p=0.024, *p=0.049).
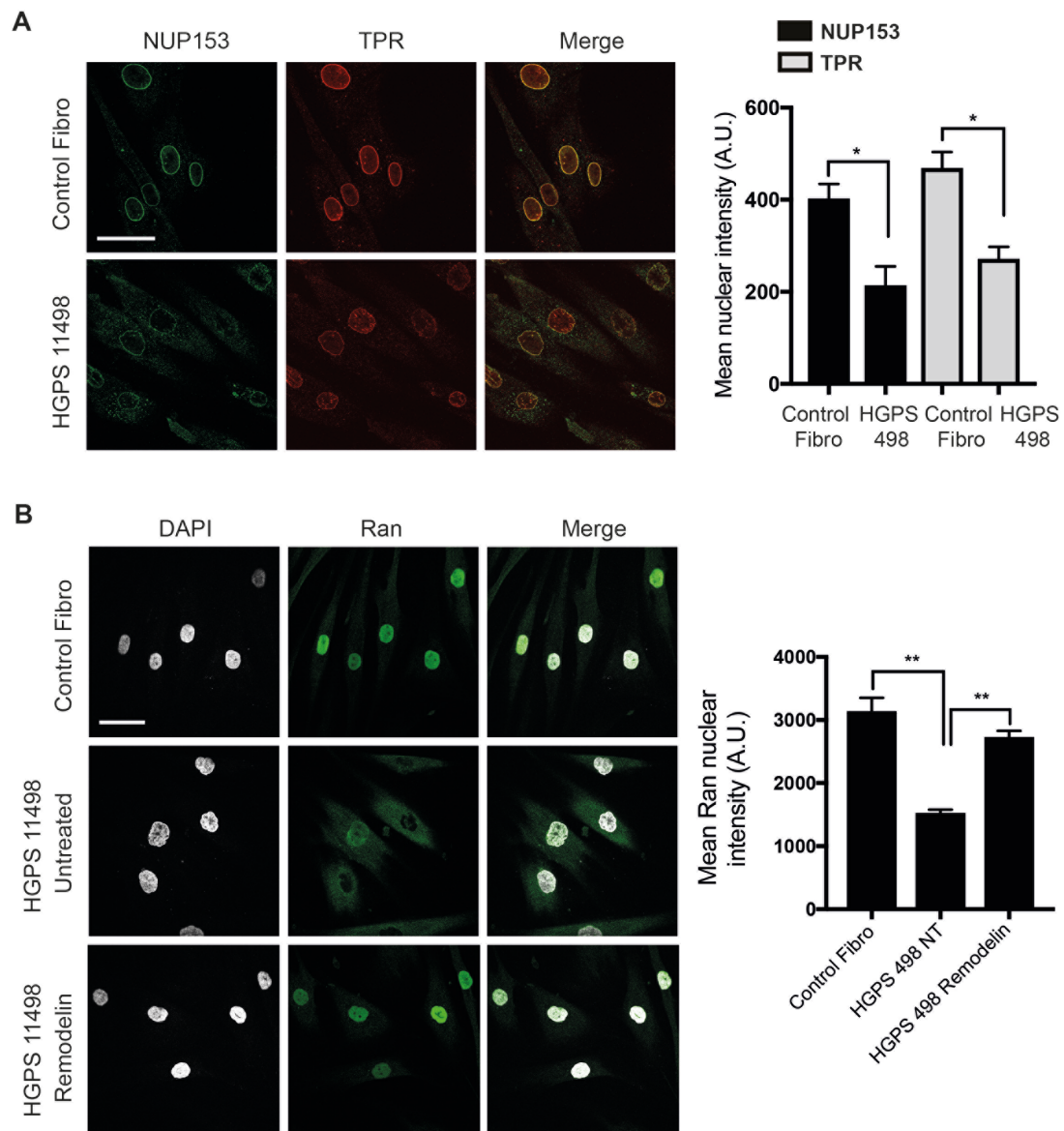
Fig. S2. Nuclear import is affected in HGPS. (**A**) Representative immunofluorescence images (left) and quantification (right) of NUP153 (green) and TPR (red) staining from three independent experiments in control fibroblasts or fibroblasts from HGPS patient 11498 (Unpaired t test, P values from left to right: *p=0.0354, *p=0.023) Error bars represent s.e.m. (**B**) Representative immunofluorescence images (left) and quantification (right) of Ran from three independent experiments in control fibroblasts or fibroblasts from HGPS patient 11498, in untreated cells or upon NAT10 inhibition by Remodelin (Unpaired t test, P values from left to right: **p=0.0092, **p=00.43). Error bars represent s.e.m. Scale bars: 50μm.
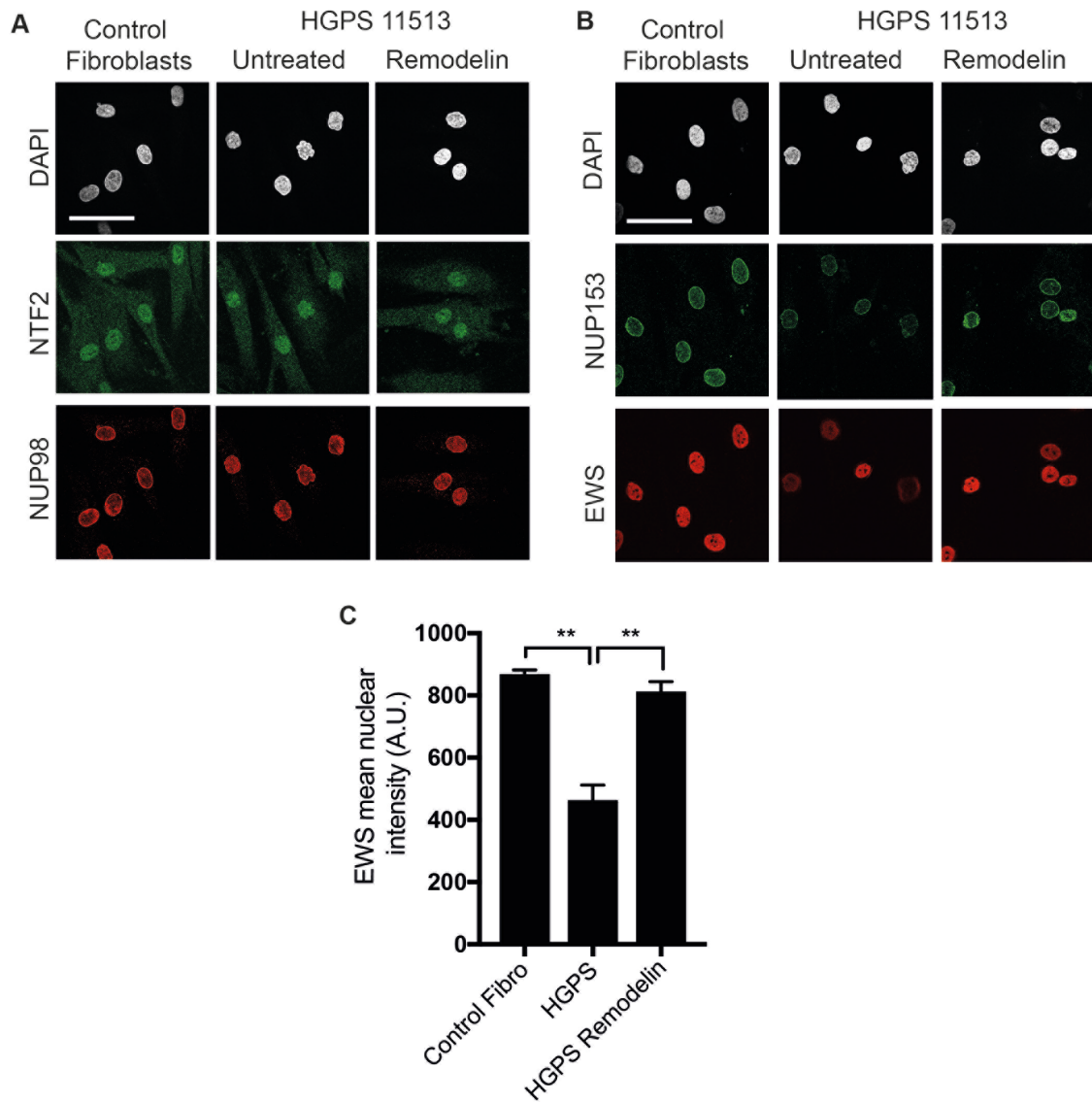
Fig. S3. TNPO1 dependent protein cargos are affected in HGPS cells. (**A**) Representative immunofluorescence images from three independent experiments showing the subcellular localisation of the NTF2 protein responsible for nuclear import of Ran. Scale bar: 50μm. (**B**) Representative immunofluorescence images from three independent experiments showing nuclear staining intensity of TNPO1 cargos including NUP153 and the Ewing sarcoma protein EWS in HGPS cells compared to controls. Scale bar: 50μm. (**C**) Quantification of EWS nuclear intensity in the indicated conditions (Unpaired t test from three independent experiments, error bars represent s.e.m. P values from left to right: **p=0.0016, **p=0.0031).
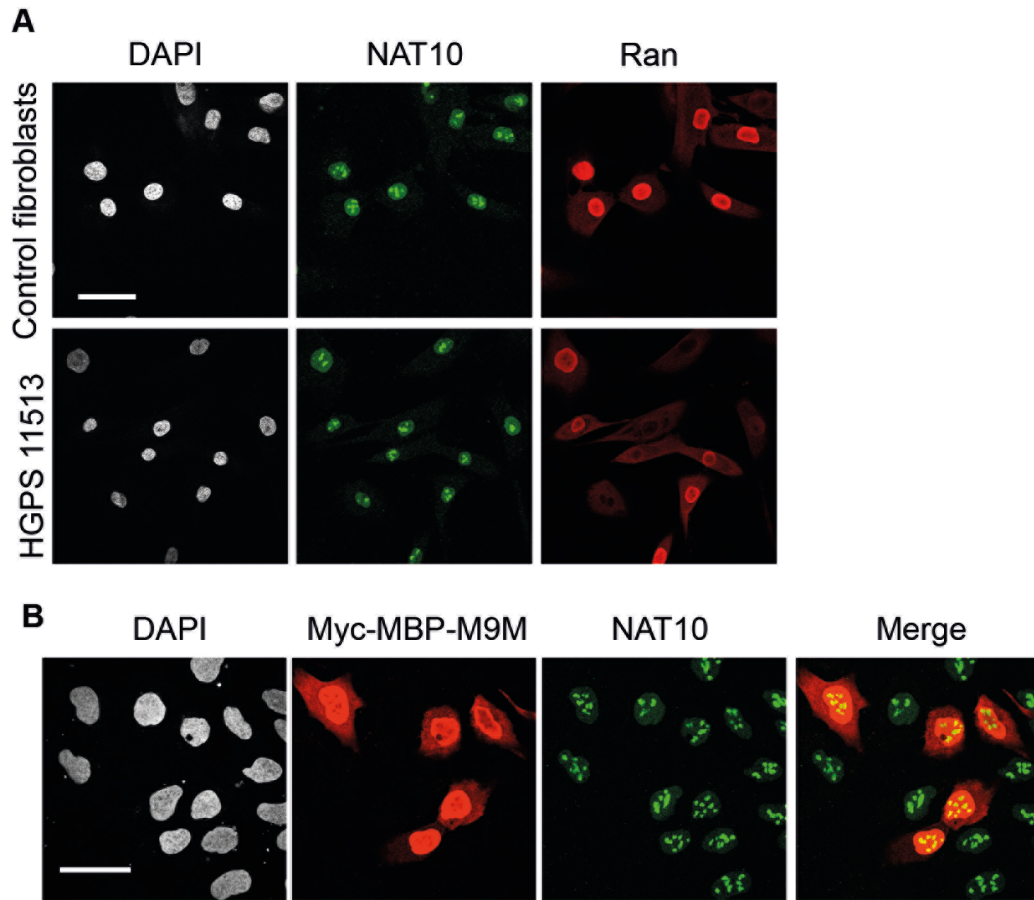
Fig. S4. NAT10 nuclear import is not dependent on TNPO1. (**A**) Representative immunofluorescence images from thee independent experiments showing NAT10 (green) and Ran (red) staining in both control and HGPS fibroblasts. Scale bar: 50μm. (**B**) Human osteosarcoma U2OS cells were transfected with the plasmid encoding the TNPO1 inhibitor Myc-MBP-M9M (40) (red) to assess the effects on NAT10 nuclear localization (green). Scale bar: 20μm.
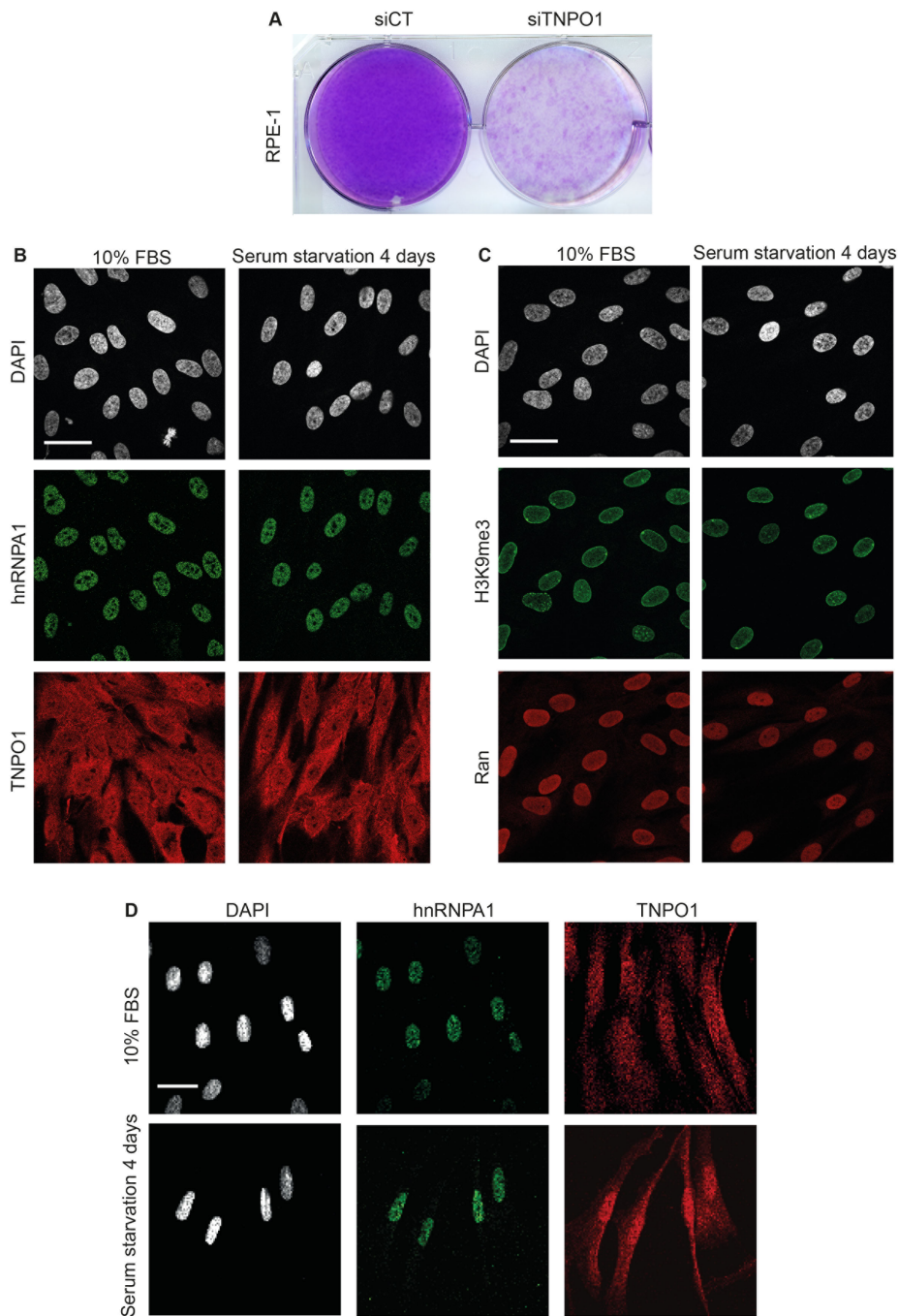
Fig. S5. Cell proliferation inhibition does not affect the Transportin-1 pathway. (A) Crystal violet staining of non-transformed human RPE-1 cells transfected with control (siCT) or TNPO1 siRNA (siTNPO1). Representative wells from three independent experiments are shown. **(B)** and **(C)** RPE-1 cells were either kept in normal or in medium without serum to arrest cell proliferation. Representative immunofluorescence images from three independent experiments showing staining of TNPO1 and its downstream cargo hnRNPA1 **(B)** as well as Ran and the heterochromatin marker H3K9me3 **(C)**. **(D)** Control fibroblasts were either kept in normal or in medium without serum to arrest cell proliferation. Representative immunofluorescence images from two independent experiments showing staining of TNPO1 and its downstream cargo hnRNPA1. Scale bars: 30μm.
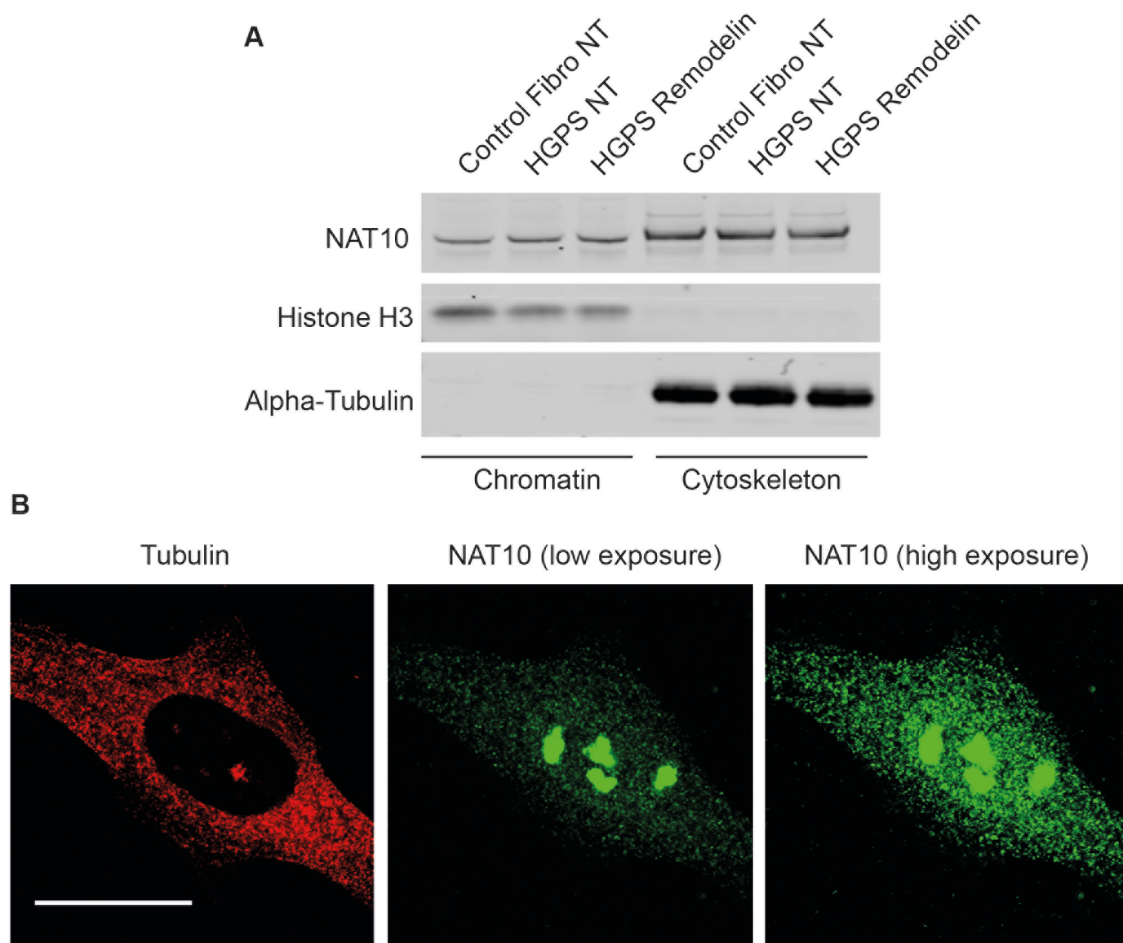
Fig. S6. NAT10 localises both in the nucleus and in the cytoskeleton. (**A**) Representative western blotting from two independent subcellular fractionations showing the abundance of the indicated proteins in the chromatin and cytoskeletal fractions of control fibroblasts and HGPS cells in the absence (non treated, NT) or presence of Remodelin. (**B**) Representative immunofluorescence images from three independent experiments showing the subcellular localisation of NAT10 upon low (middle image) or high exposure (right image). Scale bar: 10μm.
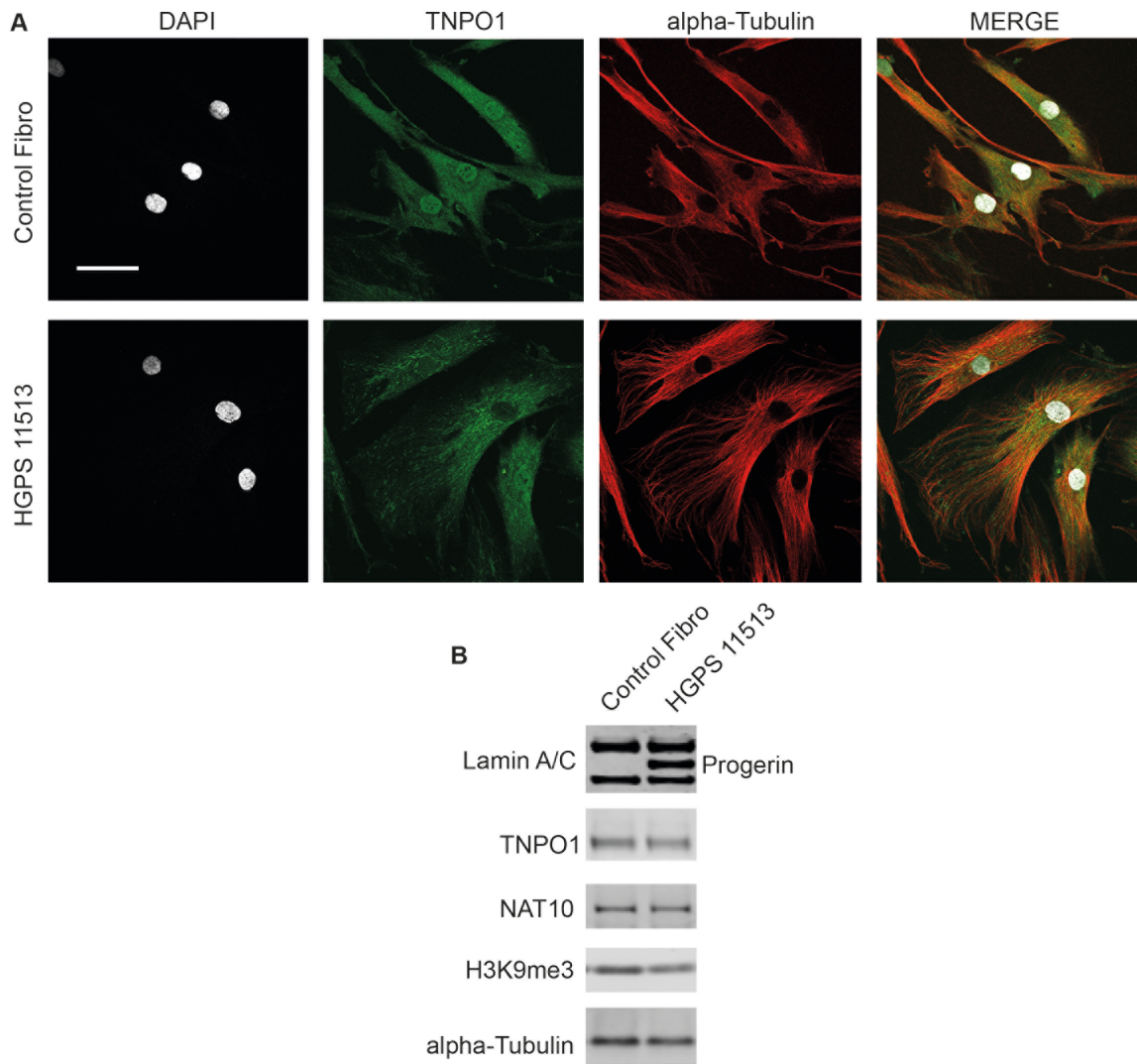
Fig. S7. TNPO1 accumulates at the microtubule network of HGPS cells. (**A**) Representative immunofluorescence images from three independent experiments showing the signal coming from the anti-TNPO1 (green) and anti-tubulin (red) antibodies used in the PLA assay. Scale bars: 50μm. (**B**) Representative Western blotting from three independent experiments showing the global abundance of the indicated proteins in control vs HGPS cells. (**C**) Immunoprecipitation of TNPO1 in control fibroblasts.
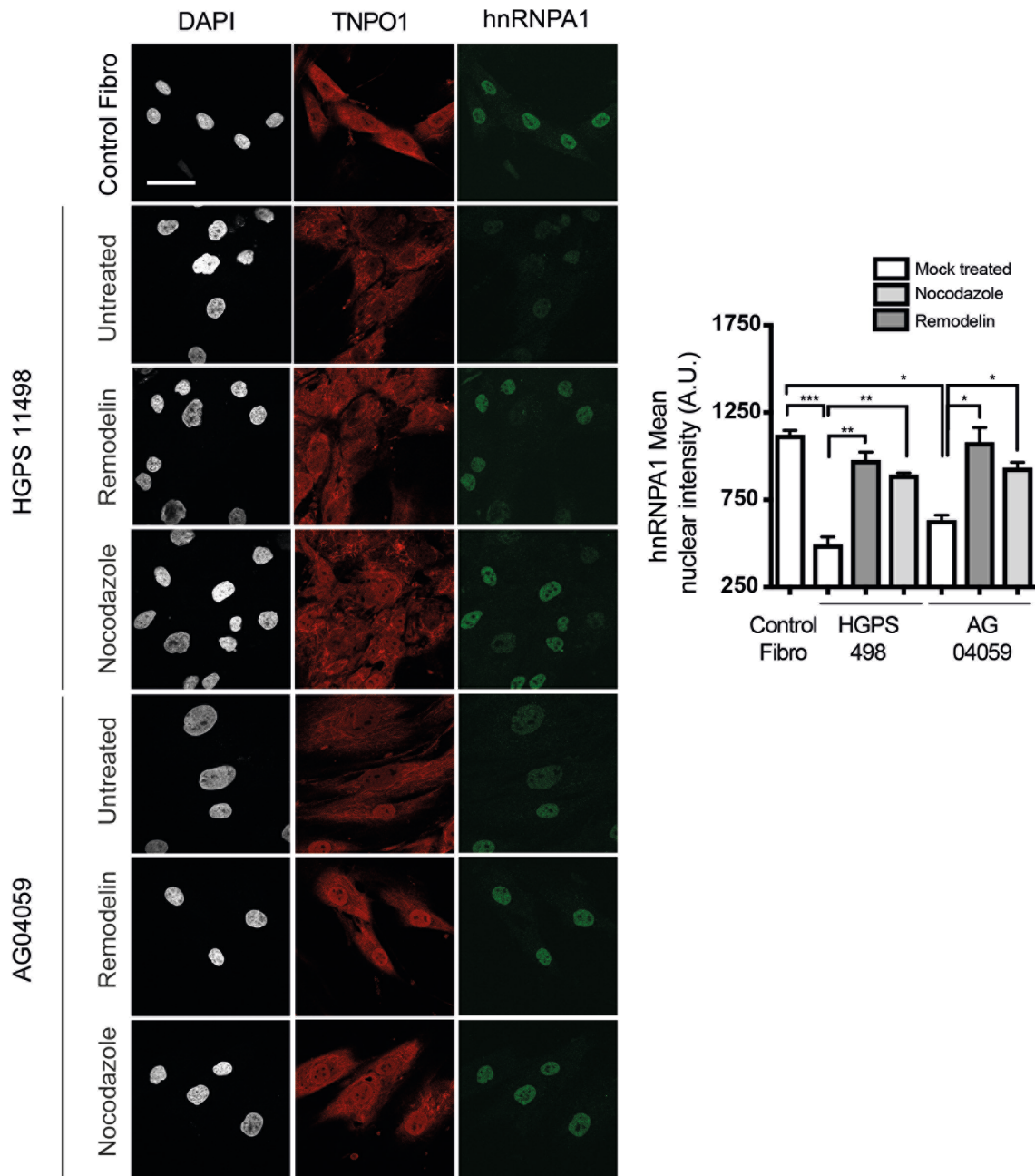
Fig. S8. TNPO1 pathway is defective in HGPS cells and in cells from aged individuals, and this is rescued by microtubule destabilization. Representative immunofluorescence images (left) and quantification (right) from three independent experiments showing nuclear staining intensity of TNPO1 (red) and hnRNPA1 (green) in HGPS (HGPS11498) and in cells from aged individual (AG04059) treated with the indicated molecules. Scale bar: 50μm. (Unpaired t test, P values from left to right: ***p=0.0001, **p=0.0069, **p=0.0081, *p=0.0128, *p=0.0420, *p=0.0253. Error bars represent s.e.m.).
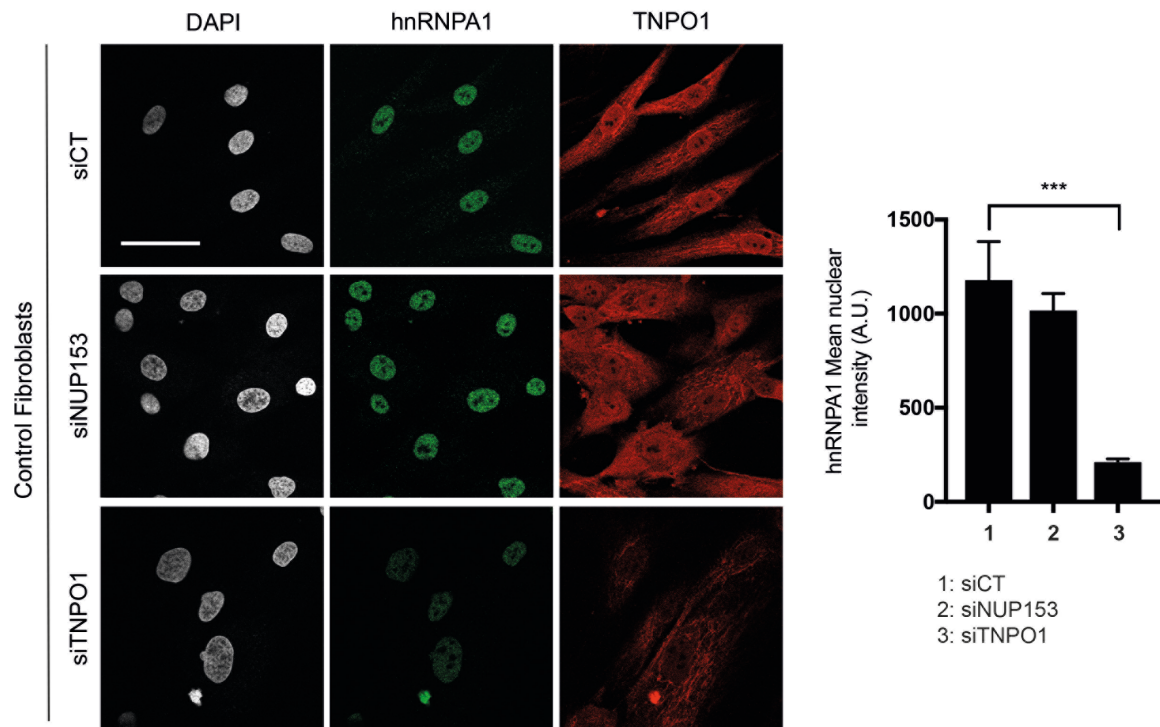
Fig. S9. NUP153 depletion does not affect the Transportin-1 pathway. Control Fibroblasts were transfected with the indicated siRNA before being stained for hnRNPA1 (green) and TNPO1 (red). Representative immunofluorescence images (left) from two independent experiments showing the effects of TNPO1 (siTNPO1) or NUP153 depletion (siNUP153) on the nuclear staining intensity of hnRNPA1. Scale bar: 50µm. Right: Quantification of hnRNPA1 nuclear intensity from two independent experiments in the indicated siRNA (Unpaired t test, P value: ***p=0.0004. Error bars represent s.e.m.).
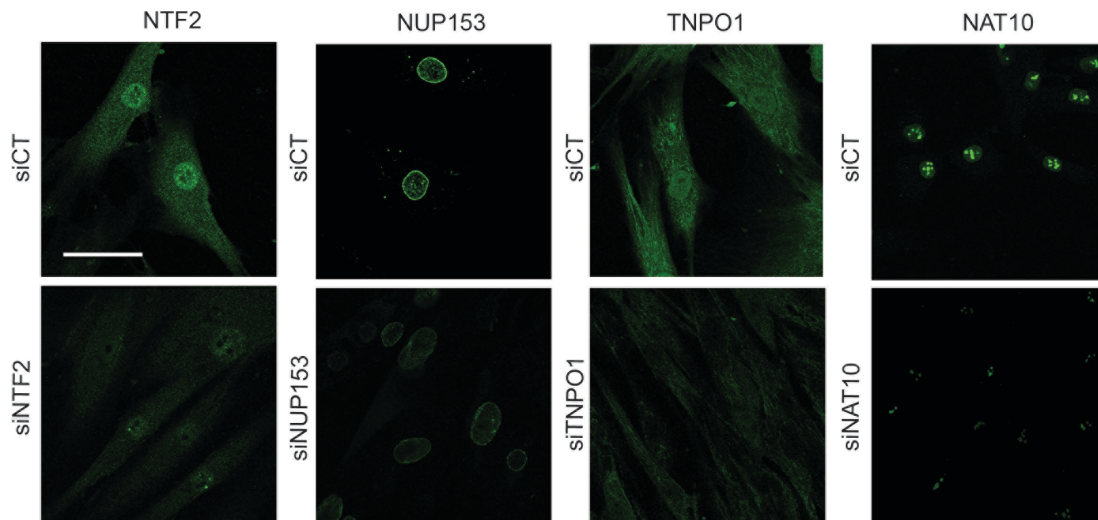
Fig. S10. Efficiency of protein depletions. The efficiency of the indicated siRNA was assessed by staining for the corresponding proteins. Representatives immunofluorescence images in control fibroblasts from three independent experiments are shown. Scale bar: 50μm.

After you've completed revising the SM legends, make sure the titles for each figure listed here match the titles in the SM list that immediately follows the Materials & Methods in the main text.

Supplementary Tables

Table S1: List of genes modified by Remodelin treatment.

This table is provided as a separate Excel file and lists the genes modified by Remodelin in control and HGPS fibroblasts.

Table S2: List of genes modified by NAT10 depletion.

This table is provided as a separate Excel file and lists the genes modified upon NAT10 depletion in control and HGPS fibroblasts.

Table S3: List of genes modified by TNPO1+NAT10 depletion.

This table is provided as a separate Excel file and lists the genes modified upon NAT10 and TNPO1 depletion in control and HGPS fibroblasts.

Table S4: List of genes modified by TNPO1 depletion.

This table is provided as a separate Excel file and lists the genes modified upon TNPO1 depletion in control and HGPS fibroblasts.

Table S5: Gene ontology analysis of "siNAT10 only" genes.

This table is provided as a separate Excel file and lists the genes modified only upon NAT10 depletion and not upon co-depletion with TNPO1 in control and HGPS fibroblasts.

Table S6. Primary antibodies used in this study.

Primary antibodies were used at the indicated concentrations for Western blotting (WB) and immunofluorescence (IF).

Antibody	Cat number	Company	Dilution WB	Dilution IF
α-tubulin	T9026	Sigma Aldrich	1/500	1/500
Histone H3	ab1791	Abcam	1/1000	N/A
H3K9me3	ab8898	Abcam	1/2000	1/1000
TPR	ab58344	Abcam	1/200	1/100
TNPO1	ab10303	Abcam	1/200	1/200
Lamin A/C	sc-6215	Santa Cruz	1/400	1/200
NAT10	13365-1-AP	ProteinTech	1/500	1/500

hnRNPA1	4296	Cell Signaling	1/100	1/50
Myc	2276	Cell Signaling	N/A	1/5000
NUP153	A301-788A	Bethyl	1/200	1/100
NUP153	MMS-102P	Covance	N/A	1/200
Ran	610341	BD Biosciences	1/500	1/200